Nucleon resonance structure in the finite volume of lattice QCD

Jia-Jun Wu,[1] H. Kamano,[2,3] T.-S. H. Lee,[4] D. B. Leinweber,[1] and A. W. Thomas[1]

[1]*Special Research Center for the Subatomic Structure of Matter (CSSM), Department of Physics,*
University of Adelaide Adelaide 5005, Australia
[2]*KEK Theory Center, Institute of Particle and Nuclear Studies (IPNS),*
High Energy Accelerator Research Organization (KEK), Tsukuba,
Ibaraki 305-0801, Japan
[3]*J-PARC Branch, KEK Theory Center, IPNS, KEK, Tokai, Ibaraki 319-1106, Japan*
[4]*Physics Division, Argonne National Laboratory, Argonne, Illinois 60439, USA*

An approach for relating the nucleon resonances extracted from πN reaction data to lattice QCD calculations has been developed by using the finite-volume Hamiltonian method. Within models of πN reactions, bare states are introduced to parametrize the intrinsic excitations of the nucleon. We show that the resonance can be related to the probability $P_{N^*}(E)$ of finding the bare state, N^*, in the πN scattering states in infinite volume. We further demonstrate that the probability $P_{N^*}^V(E)$ of finding the same bare states in the eigenfunctions of the underlying Hamiltonian in finite volume approaches $P_{N^*}(E)$ as the volume increases. Our findings suggest that the comparison of $P_{N^*}(E)$ and $P_{N^*}^V(E)$ can be used to examine whether the nucleon resonances extracted from the πN reaction data within the dynamical models are consistent with lattice QCD calculation. We also discuss the measurement of $P_{N^*}^V(E)$ directly from lattice QCD. The practical differences between our approach and the approach using the Lüscher formalism to relate LQCD calculations to the nucleon resonance poles embedded in the data are also discussed.

I. INTRODUCTION

One of the most challenging problems in modern hadron physics is to understand the spectra of baryons and mesons within quantum chromodynamics (QCD), the fundamental theory of the strong interactions. It is therefore important to investigate how the properties of the excited nucleons can be understood using lattice QCD calculations (LQCD). Important progress in this direction has been made in recent years [1,2] and the accuracy of the results is expected to improve rapidly in the near future. It is therefore necessary to address the question of how LQCD results can be related to the experimental data and, further, how they may be used to understand the manner in which nucleon excited states emerge from nonperturbative QCD.

The excited nucleons are unstable and coupled with the meson-nucleon continuum to form nucleon resonances (N^*). Thus the properties of excited nucleons can only be studied by analyzing the nucleon resonances extracted from data, such as meson production reactions induced by pions, photons and electrons. Accordingly, it is necessary to develop an approach to relate the resonance parameters, which are defined on the complex energy (E) plane, to the results from LQCD calculations. The main progress was made by Lüscher in Refs. [3,4], where an equation connecting the spectra in a finite volume and the phase shift and inelasticity in infinite volume was developed. Based on these papers, there has been a great deal of work extending the Lüscher formalism to the two-body coupled-channel case [5–11]. A review of recent progress may be found in Ref. [12].

As pointed out in Refs. [13–15], the equation connecting the S matrix and the energy levels presents difficulties in the practical application in the multichannel case, even for the one-channel case with higher partial waves. In the multichannel case, there are N free parameters in the S matrix for a single energy level. For example, there are $N = 3$ parameters, two phase shifts and one inelasticity, for two coupled channels. Thus, to extract these N parameters of fixed energy, one needs N independent equations with different lattice sizes at this energy. That is, we need to find several different lattice sizes which produce the same energy eigenvalue. Unfortunately, it is hard to collect several lattice sizes with the same energy eigenvalue because the time consuming generation of lattice configurations needs to be done separately for each lattice size. On the other hand, if we expect to predict the spectra in the finite volume with fixed size, the full S matrix is required. However, as we know, the experimental data only can provide the phase shifts and inelasticities for a few channels. For example, for the $f_0(980)$ resonance, there are very limited data for the phase shifts in the $K\bar{K}$ channel. In summary, although the equation does provide a reliable relationship between the S matrix and the energy levels, it is hard to apply only because of the limited experimental data and lattice results available. For clarification, a detailed discussion will be presented in Sec. IV. Thus, in order to avoid this problem, we need to introduce a parametrization method to complete the analysis and predict the spectra in the lattice finite volume. For example, in Refs. [14,16], the

K-matrix model is applied. However, there are other approaches which do not directly use these equations generated from the Lüscher formalism. There, the energy levels in the finite volume are calculated from the eigenvalues of a finite volume Hamiltonian matrix [15,17–21]. Alternatively, the pole positions of the finite volume T matrix [22–25] provide the finite volume energies. Both of these methods have been shown to be consistent with the Lüscher formalism up to exponentially suppressed corrections [15,22].

In the first approach [14,16,26,27], they combine the K-matrix model with the Lüscher formalism. Of course, one can also use other models to generate the S matrix. First, by controlling the parameters in the K-matrix model, the full S matrix is generated. Then the spectra in the finite volume can be calculated through the Lüscher formalism with the input of the full S matrix. Thirdly by fitting the spectra measured in the lattice, the parameters in the model will be determined; i.e., the K-matrix model is fixed by fitting the spectra in the finite volume. In the last step, resonance parameters extracted within the constructed K-matrix model are then compared with those listed by the Particle Data Group (PDG) [28].

The second approach is the finite-volume Hamiltonian (FVH) method developed in Refs. [15,17–21,29]. This starts with the construction of a Hamiltonian to fit the data of the processes under consideration. The resulting Hamiltonian is then used to predict the spectrum in finite volume and that is compared with the spectrum calculated from LQCD. Agreement between these spectra implies that the LQCD calculation gives the same resonance parameters embedded in the data through the constructed Hamiltonian. Alternatively, this second approach can also be used to fit the LQCD energy spectrum and the resulting Hamiltonian can then be used to calculate phase shifts for comparison with experimental data. In the process of calculating the finite volume spectrum, one gains insight into the composition of the lattice QCD eigenstates. One can examine the eigenvectors of correlation matrices constructed from single-particle and multiparticle interpolating fields. The main task of this paper is to draw on this information and connect this insight directly to the basis states of the model. From the Hamiltonian model, we can not only describe the spectrum in the finite volume, but also the components of these eigenstates.

We emphasize the difference from the first approach discussed above. In the FVH method, we are also examining the eigenvectors of the Hamiltonian model and their direct connection to the lattice QCD eigenstates, a connection that cannot be made through an intermediary infinite volume scattering amplitude. It is important to build a bridge between models and lattice results directly, rather than through the S matrix, because the lattice produces more information than the S matrix alone.

The approach developed in Refs. [22–25] also involves a formulation of the problem within a finite volume, starting with the scattering equations deduced from unitarized chiral perturbation theory. It has also been used to extract resonance parameters by an appropriate analytic continuation.

If the spectrum calculated from LQCD is of very high accuracy and covers a sufficiently wide energy region, within which the experimental data for investigating a particular nucleon resonance are also accurate and complete (as reviewed in Ref. [30]), then the first and second approaches are equally valid. This is supported by the results from a study [31] of resonance extractions and the FVH method. It was demonstrated within several exactly soluble models that the extracted resonance parameters are independent of the model used in the resonance extraction as far as the partial-wave amplitude data within the sufficiently wide region near the considered resonance are fitted *precisely* (i.e., within 1% considered in Ref. [31]).

Unfortunately, this ideal situation does not exist in reality for investigating nucleon resonances at the present time. The scattering amplitudes determined from either the experimental data or the LQCD spectrum and Lüscher's formula have intrinsic errors associated with the unavoidable systematic and statistical errors. Thus the extracted resonance parameters, widths and residues, can depend significantly on the parametrization of the K-matrix and the form of the Hamiltonian used to fit the determined scattering amplitudes within the errors, particularly in the higher-mass region as observed in Ref. [32].

The purpose of the present work is to apply the FVH method in the development of an approach to relate the nucleon resonances to LQCD calculations. Instead of the separable potential models used in the previous FVH studies [15,17–19], dynamical πN reaction models based on meson-exchange mechanisms are used. We will start with a one-channel dynamical model [the Sato-Lee (SL) model] developed in Ref. [33]. This model, with one bare state in the P_{33} partial wave, is consistent with the well-accepted interpretation [34,35] that the Δ (1232) resonance is made of a quark core and a meson cloud.

We first apply the SL Hamiltonian to confirm the results, as established in [15,17–21], that the FVH method is equivalent to using Lüscher's formalism in relating the spectrum in finite volume to the scattering amplitudes in infinite volume. We then observe that the probability $P_{\Delta}(E)$ of finding the bare Δ state in the πN scattering wave function contains resonance information which can be verified on the real-E axis, which is in turn accessible to experiments. We then demonstrate that an energy-averaged probability $P_{\Delta}^{V}(E, L)$ of finding the bare Δ in the eigenstate of the Hamiltonian in finite volume approaches $P_{\Delta}(E)$ as the volume size L increases. This result indicates that $P_{\Delta}^{V}(E, L)$ from LQCD calculations can be related directly to the nucleon resonance information extracted within the given dynamical model. Clearly, this is rather different from Approach 1 mentioned above, which uses the K-matrix model to extract nucleon resonance properties from the

spectrum obtained in LQCD calculations. In addition, the authors of Refs. [36,37], developed another method for extracting the Breit-Wigner form of resonances from the lattice spectrum. The differences between their approach and that presented here are discussed in Sec. III.

We next consider a three-channel, meson-exchange πN model. The parameters of this model are determined by fitting the empirical S- and P-wave amplitudes up to $W = 1.6$ GeV. This allows us to examine the more complex situations, in which the multichannel system is considered, and two resonances are associated with the same bare state in the P_{11} partial wave. This is similar to the results obtained from the analysis of Ref. [32]. Here we examine closely the differences between using the FVH method and Lüscher's formalism to relate the multichannel scattering amplitudes and the associated nucleon resonances to the LQCD calculations through the spectrum in finite volume. We then demonstrate that for the multichannel case the probability $P_\Delta^V(E, L)$ in finite volume also approaches the probability $P_\Delta(E)$ in infinite volume, as the volume increases.

Our findings suggest that the comparison of $P_{N^*}(E)$ and $P_{N^*}^V(E, L)$ can be used to examine whether the nucleon resonances extracted from the πN reaction data within the dynamical models are consistent with LQCD. We will discuss possible LQCD calculations of $P_{N^*}^V(E, L)$ for interpreting the bare states of the dynamical models. This provides a new method to extract the properties of hadrons directly from LQCD calculations through measuring $P_{N^*}^V(E, L)$. We anticipate the formalism developed herein will be applied in next-generation lattice QCD calculations extracting the complete spectrum through the incorporation of nonlocal meson-baryon interpolating fields.

In Sec. II, we present details of the calculations based on a dynamical Hamiltonian model in infinite volume and in a finite volume. The results for the SL model and the three-channel model are presented in Secs. III and IV, respectively. In Sec. V and Appendix A, we discuss possible LQCD calculations of $P_{N^*}^V(E, L)$. A summary and some discussion of possible future directions are given in Sec. VI.

II. SCATTERING SOLUTIONS FROM DYNAMICAL HAMILTONIANS

The Hamiltonian of the dynamical model we will consider is defined by

$$H = H_0 + H_I, \qquad (1)$$

where H_0 is the free Hamiltonian.

The interaction Hamiltonian is taken to have the following form,

$$H_I = \sum_{i=1,n_c} g_{N^*,i} + \sum_{i,j=1,n_c} v_{i,j}, \qquad (2)$$

where n_c is the number of meson-baryon channels considered; $g_{N^*,i}$ is the vertex interaction defining the decay of

a bare state, $|N_C^*\rangle$, into the ith meson-baryon channel; and $v_{i,j}$ is the two-body meson-baryon interaction between channels i and j.

In both the SL model and the three-channel model, the interactions $v_{i,j}$ are calculated from meson-exchange mechanisms derived from phenomenological Lagrangians. The bare state introduced here is a renormalization scheme dependent quantity and consequently unphysical. The merit of working with the bare state quantity is in selecting a renormalization scheme of relevance to the legacy of phenomenological approaches to understand the resonance structure. In our case, physicists studying QCD resonance structure adopt form factors that describe the finite size of the meson-cloud source. These practitioners are thus interested in the effective field theory results when the regulator parameter of the effective field theory is taken to be a dipole with scale of order 1 GeV, which produces excellent phenomenology. And while the bare state is not physical, it is still of interest to the field as it gives important insight into how QCD gives rise to resonance structure.

In the following two subsections, we write down the formulas required to calculate the scattering amplitudes from the Hamiltonian Eqs. (1) and (2) in infinite volume as well as in finite volume.

A. Solutions in infinite volume

Based on the Hamiltonian defined by Eqs. (1) and (2), it is known [32,33] that the scattering amplitudes of each partial wave can be written as

$$T_{i,j}(k, k'; E) = t_{i,j}^{\text{bg}}(k, k'; E) + t_{i,j}^{\text{res}}(k, k'; E). \qquad (3)$$

Here and in the rest of this paper the indices (i, j) also specify the quantum numbers associated with the meson-baryon channel, namely, the orbital angular momentum (L), total spin (S), total angular momentum (J), parity (P), and isospin (I). The "background" amplitudes $t_{i,j}^{\text{bg}}(k, k', E)$ are calculated from the meson-baryon interactions by

$$\begin{aligned} t_{i,j}^{\text{bg}}(k, k'; E) &= v_{i,j}(k, k'; E) \\ &+ \sum_m \int k''^2 dk'' v_{i,m}(k', k''; E) \\ &\times \frac{1}{E - E_{M_m}(k'') - E_{B_m}(k'') + i\epsilon} \\ &\times t_{m,j}^{\text{bg}}(k'', k'; E). \end{aligned} \qquad (4)$$

The resonant amplitudes are

$$t_{i,j}^{\text{res}}(k, k'; E) = \frac{\bar{\Gamma}_i^\dagger(k; E) \bar{\Gamma}_j(k'; E)}{E - m_0 - \Sigma(E)}, \qquad (5)$$

where the dressed vertex functions are

$$\bar{\Gamma}_i^\dagger(k; E) = \Gamma_i^\dagger(k) + \sum_m \int k'^2 dk' t_{i,m}^{bg}(k, k'; E)$$

$$\times \frac{1}{E - E_{M_m}(k') - E_{B_m}(k') + i\epsilon} \Gamma_m^\dagger(k'), \qquad (6)$$

$$\bar{\Gamma}_j(k; E) = \Gamma_j(k) + \sum_m \int k'^2 dk' \Gamma_m(k')$$

$$\times \frac{1}{E - E_{M_m}(k') - E_{B_m}(k') + i\epsilon} t_{m,j}^{bg}(k', k; E), \qquad (7)$$

and the self-energy of the N^* is

$$\Sigma(E) = \sum_m \int k'^2 dk' \Gamma_m(k')$$

$$\times \frac{1}{E - E_{M_m}(k') - E_{B_m}(k') + i\epsilon} \bar{\Gamma}_m^\dagger(k'; E). \qquad (8)$$

As developed in Refs. [38,39], the resonance poles E_{res} of the scattering amplitudes $T_{i,j}$ can be found from the resonant part $t_{i,j}^{res}$ of Eq. (3). From the expression Eq. (5), it is clear that E_{res} can be obtained by solving the following equation on the complex E plane:

$$E_{res} - m_0 - \Sigma(E_{res}) = 0. \qquad (9)$$

This equation can lead to many poles. However, only the poles near the physical region are relevant to the physical observables. The energies of these resonance poles in general have the form $E_{res} = E_R - iE_I$ with $E_R, E_I > 0$. In the Argonne National Laboratory–Osaka University (ANL-Osaka) analysis [32], only those poles with $E_I < 200$ MeV are considered to be related to excited nucleon states through their coupling with the meson-baryon continuum.

We next use $t_{\pi N, \pi N}^{res}$ of the total amplitude T of Eq. (3) to define the resonant cross section of πN elastic scattering as

$$\sigma^{res}(E) = \frac{(4\pi)^2}{k_{\pi N}^2} \rho_{\pi N}^2(E) \frac{2J+1}{2} |t_{\pi N, \pi N}^{res}(k_{\pi N}, k_{\pi N}, E)|^2,$$

$$= \frac{(4\pi)^2}{k_{\pi N}^2} \rho_{\pi N}^2(E) \frac{2J+1}{2} \left| \frac{\bar{\Gamma}_{\pi N}^\dagger(k_{\pi N}; E) \bar{\Gamma}_{\pi N}(k_{\pi N}; E)}{E - m_0 - \Sigma(E)} \right|^2, \qquad (10)$$

where $k_{\pi N}$ is the πN on-shell momentum, and $\rho_{\pi N}(E) = \pi k_{\pi N} E_N(k) E_\pi(k)/E$. We can cast Eq. (10) into the following form:

$$\sigma^{res}(E) = \left| \frac{1}{E - m_0 - \Sigma(E)} \right|^2$$

$$\times \left[\frac{(4\pi)^2}{k_{\pi N}^2} \rho_{\pi N}^2(E) \frac{2J+1}{2} |\bar{\Gamma}_{\pi N}(k_{\pi N}, ; E)|^4 \right]. \qquad (11)$$

Because of the condition Eq. (9), one can consider that $\sigma_{\pi N}^{res}(E)$ contains the resonance information on the real-E axis which is accessible to experiments. In some cases it is possible to cast the expression Eq. (11) into the Breit-Wigner form in the region where $(E_R - 2E_I) \leq E \leq (E_R + 2E_I)$. But the parameters of the resulting Breit-Wigner resonances will differ from those of the extracted resonance poles, which are known [38,40] to be the energies of the eigenstates of the underlying Hamiltonian with an outgoing wave boundary condition.

We now introduce a quantity which can be related to σ^{res} and which can also be defined within the finite-volume formulation. We start by examining the scattering wave function with an incident plane-wave state in the $i = 1 = \pi N$ channel. It is defined by the total amplitude Eq. (3):

$$|\Psi_{E,\pi N}^{(+)}\rangle = \left[1 + \frac{1}{E - H_0 + i\epsilon} T(E)\right] |k_{\pi N}\rangle, \qquad (12)$$

where $|k_{\pi N}\rangle$ is the incoming πN plane-wave state. It is well known from standard reaction theory [41] that

$$(H_0 + H_I)|\Psi_{E,\pi N}^{(+)}\rangle = E|\Psi_{E,\pi N}^{(+)}\rangle. \qquad (13)$$

We can use the definition Eq. (12) and the solutions given by Eqs. (3)–(8), to verify Eq. (13) explicitly and also to obtain the following relation:

$$\langle N_C^* | \Psi_{E,\pi N}^{(+)} \rangle = \frac{\bar{\Gamma}_{\pi N}(k_{\pi N}; E)}{E - m_0 - \Sigma(E)}. \qquad (14)$$

Thus the probability of finding the bare state $|B\rangle$ in the πN scattering wave function is

$$p_{\pi N}(E) = |\langle N_C^* | \Psi_{E,\pi N}^{(+)} \rangle|^2 = \left| \frac{\bar{\Gamma}(k_{\pi N}; E)}{E - m_0 - \Sigma(k)} \right|^2. \qquad (15)$$

By comparing $p_{\pi N}(E)$ and $\sigma^{res}(E)$ [Eq. (11)], we can see that $p_{\pi N}(E)$ contains the resonance information on the real-E axis which is accessible to experiments.

One can generalize the above formula to define $p_i(E)$ for any channel $i = 1, \ldots, n_c$ included in the model. We define the total probability of finding the bare N^* state in the scattering wave function as

$$P_{N_C^*}(E) = \frac{1}{Z} \left[\sum_{i=1, n_c} \rho_i(E) p_i(E) \right], \qquad (16)$$

with

$$\rho_i(E) = \pi k_i E_{M_i}(k_i) E_{B_i}(k_i), \qquad (17)$$

where k_i is the on-shell momentum of channel i, and

$$p_i(E) = |\langle B | \Psi_{E,i}^{(+)} \rangle|^2, \tag{18}$$

$$= \left| \frac{\bar{\Gamma}(k_i; E)}{E - m_0 - \Sigma(E)} \right|^2, \tag{19}$$

$$Z = \sum_{i=1,n_c} \int_{E_{th_i}}^{\infty} dE \rho_i(E) p_i(E). \tag{20}$$

Here E_{th_i} is the threshold energy in the ith channel. Clearly, we can write

$$P_{N_C^*}(E) = \left| \frac{1}{E - m_0 - \Sigma(E)} \right|^2 \frac{1}{Z} \sum_i \rho_i(E) |\bar{\Gamma}_i(k_i, E)|^2. \tag{21}$$

By comparing Eqs. (11) and (21), we observe that $P_{N_C^*}(E)$ has a similar energy dependence to $\sigma^{\mathrm{res}}(E)$ and that it also contains the resonance information on the real-E axis which is accessible to experiments.

B. Solution in a finite volume

In a periodic volume characterized by side length L, the quantized three-momenta of mesons and baryons must be $k_n = \sqrt{n} \frac{2\pi}{L}$ for integers $n = 0, 1, 2, \ldots$ Because of the presence of a bare state $|N_C^*\rangle$ in the dynamical Hamiltonian Eqs. (1) and (2), the wave function $|\Psi_E^V\rangle$ obtained by solving the Schrödinger equation in finite volume must be of the following form:

$$|\Psi_E^V\rangle = |N_C^*\rangle \langle B | \Psi_E^V \rangle + \sum_{i=1,n_c} \sum_{n_i=0,N-1} |k_{n_i}\rangle \langle k_{n_i} | \Psi_E^V \rangle, \tag{22}$$

where $|k_0\rangle, |k_1\rangle, \ldots, |k_{N-1}\rangle$ are the plane-wave states for a given choice of N momenta and n_c is the number of meson-baryon channels considered. Solving the Schrödinger equation

$$(H_0 + H_I)|\Psi_E^V\rangle = E|\Psi_E^V\rangle, \tag{23}$$

in finite volume is then equivalent to finding the eigenvalues of the following matrix equation,

$$\det([H_0]_{N_c+1} + [H_I]_{N_c+1} - E[I]_{N_c+1}) = 0, \tag{24}$$

where $[I]_{N_c+1}$ is an $(N_c+1) \times (N_c+1)$ unit matrix with $N_c = N \times n_c$.

The matrix for the free Hamiltonian in Eq. (24) takes the following form,

$$[H_0]_{N_c+1} = \begin{pmatrix} m_0 & 0 & 0 & \cdots & 0 & 0 & \cdots \\ 0 & \epsilon_1(k_0) & 0 & \cdots & 0 & 0 & \cdots \\ 0 & 0 & \epsilon_2(k_0) & \cdots & 0 & 0 & \cdots \\ 0 & 0 & 0 & \ddots & 0 & 0 & \cdots \\ 0 & 0 & 0 & \cdots & \epsilon_{n_c}(k_0) & 0 & \cdots \\ 0 & 0 & 0 & \cdots & 0 & \epsilon_1(k_1) & \cdots \\ \vdots & \vdots & \vdots & \vdots & \vdots & \vdots & \ddots \end{pmatrix},$$

where m_0 is the mass of the bare N^* state, and

$$\epsilon_i(k_n) = E_{M_i}(k_n) + E_{B_i}(k_n). \tag{25}$$

Here $E_{M_i}(k_n)$ and $E_{B_i}(k_n)$ are the free energies of the meson (M) and baryon (B) in the ith channel, respectively. The $(N_c+1) \times (N_c+1)$ matrix for the interaction Hamiltonian Eq. (2) is

$$[H_I]_{N_c+1} = \begin{pmatrix} 0 & g_1^V(k_0) & g_2^V(k_0) & \cdots & g_{n_c}^V(k_0) & g_1^V(k_1) & \cdots \\ g_1^V(k_0) & v_{1,1}^V(k_0,k_0) & v_{1,2}^V(k_0,k_0) & \cdots & v_{1,n_c}^V(k_0,k_0) & v_{1,1}^V(k_0,k_1) & \cdots \\ g_2^V(k_0) & v_{2,1}^V(k_0,k_0) & v_{2,2}^V(k_0,k_0) & \cdots & v_{2,n_c}^V(k_0,k_0) & v_{2,1}^V(k_0,k_1) & \cdots \\ \vdots & \vdots & \vdots & \ddots & \vdots & \vdots & \cdots \\ g_{n_c}^V(k_0) & v_{n_c,1}^V(k_0,k_0) & v_{n_c,2}^V(k_0,k_0) & \cdots & v_{n_c,n_c}^V(k_0,k_0) & v_{n_c,1}^V(k_0,k_1) & \cdots \\ g_1^V(k_1) & v_{1,1}^V(k_1,k_0) & v_{1,2}^V(k_1,k_0) & \cdots & v_{1,n_c}^V(k_1,k_0) & v_{1,1}^V(k_1,k_1) & \cdots \\ \vdots & \vdots & \vdots & \vdots & \vdots & \vdots & \ddots \end{pmatrix}, \tag{26}$$

with

$$g_i^V(k_n) = \sqrt{\frac{C_3(n)}{4\pi}} \left(\frac{2\pi}{L}\right)^{3/2} g_{B,i}(k_n), \tag{27}$$

$$v_{i,j}^V(k_{n_i}, k_{n_j}) = \sqrt{\frac{C_3(n_i)}{4\pi}} \sqrt{\frac{C_3(n_j)}{4\pi}} \left(\frac{2\pi}{L}\right)^3 v_{i,j}(k_{n_i}, k_{n_j}), \tag{28}$$

where $C_3(n)$ is the number of degenerate states with the same magnitude $k_n = |\vec{k}_n|$. By solving Eq. (24), we then obtain the spectrum $(E_1, E_2, \ldots)$ for each partial wave and the corresponding wave function of the eigenstate $|\Psi_{E_i}^V\rangle$.

In practice, we follow Refs. [15,17] in using the partial-wave matrix elements of $g_{B,i}$ and $v_{i,j}$ to solve Eqs. (24)–(28). Thus the spin information of particles is already included in the Hamiltonian matrix, which is of the same form as for spinless particles. Because the symmetry of the SO(3) group in the infinite volume is reduced to the cubic group in the lattice, the irreducible representations of the cubic group will mix the high partial waves with the low partial waves. For the P_{33} and P_{11} cases in the rest frame, the next mixing partial waves are E wave ($L = 3$) of the πN and $\pi \Delta$ channels and F wave ($L = 4$) for the σN channel [4], respectively. Such high partial waves will be suppressed with the factor k_{cm}^{2l+1} in the threshold regime, where k_{cm} is the momentum of each particle in the center of mass system. On the other hand, we also do not have experimental data input for such high partial waves to constrain the parameters. Based on these considerations, we cut the partial waves at $L = 2$. Furthermore, for the simplification of the labeling, we still use the labels of P_{33} and P_{11} in the finite volume. Accordingly, we only consider the pure P-wave contributions in the calculations of the spectra for the P_{33} channels. With these simplifications, only the zeta function $Z_{00}(1, q^2)$ is needed to use the Lüscher formula to calculate the phase shifts from the predicted spectrum, as described below. The validity of this procedure has been established in Refs. [15,17].

For the single channel $n_c = 1$ case, the Lüscher [4] formalism gives a phase shift $\delta(E)$ for each energy E of the predicted spectrum by

$$\delta(E) = -\tan^{-1}\left(-\frac{q\pi^{3/2}}{Z_{00}(1; q^2)}\right) + n\pi \qquad (29)$$

where $q = \frac{kL}{2\pi}$ is evaluated in terms of the three-momentum k for the energy $E = E_N(k) + E_\pi(k)$ of the spectrum, and $Z_{00}(1; q^2)$ is the generalized zeta function. The formalism for two channels was developed in Ref. [7] and for the general multichannel case in Ref. [8].

With the eigenstate $|\Psi_{E_\alpha}^V\rangle$ (spin index omitted) in the rest frame of the N^*, which is of the form of Eq. (22), from solving Eq. (24), we can calculate the probability of finding the bare state N^*:

$$p_{N_C^*}^V(E_\alpha, L) = |\langle N_C^* | \Psi_{E_\alpha}^V \rangle|^2. \qquad (30)$$

As we will show explicitly in Sec. III, $p_{N_C^*}^V(E_\alpha)$ is not a smooth function of E_α. We therefore define the following energy-averaged form,

$$P_{N_C^*}^V(E_k^{ave}, \Delta E, L) = \frac{1}{Z^V}\frac{1}{\Delta E}\left[\sum_{E_k^{ave}-\frac{\Delta E}{2}\leq E_\alpha \leq E_k^{ave}+\frac{\Delta E}{2}} p_{N_C^*}^V(E_\alpha, L)\right],$$

$$(31)$$

where

$$Z^V = \sum_\alpha p_{N_C^*}^V(E_\alpha, L), \qquad (32)$$

which averages over states within a range ΔE centered at E_k^{ave}. From the above definitions, we have

$$\sum_{k=1,N_E} P_{N_C^*}^V(E_k^{ave}, L)\Delta E = 1, \qquad (33)$$

where N_E is the number of values, $(E_1^{ave}, E_2^{ave}, \ldots)$, chosen in the range of the predicted spectrum used to obtain the energy-averaged values. Obviously, $P_{N_C^*}^V(E_k^{ave}, L)$, as defined in Eq. (31), can have a well-defined dependence on E_k^{ave} only when there exist values of E_i to cover the interval ΔE for each chosen E_k^{ave}. From the spectrum calculated as a function of L, as will be shown in Figs. 2 and 7, it is straightforward to see that a larger L is required in order to have a smooth $P_{N_C^*}^V(E_k^{ave}, L)$, with a small ΔE. Obviously, extremely small ΔE will make $P_{N_C^*}^V(E_k^{ave}, L)$ the same as $p_{N_C^*}^V(E_\alpha)$ with an overall factor. Thus, in order to keep the $P_{N_C^*}^V(E_k^{ave}, L)$ smoothly, ΔE cannot be too small. In the calculations to be presented in the next two sections, we find that $L \times \Delta E \sim 4$ will yield a well-defined function of $P_{N_C^*}^V(E_k^{ave}, L)$. With this relation in mind, we simplify our notation for $P_{N_C^*}^V(E, \Delta E, L)$ to $P_{N_C^*}^V(E, L)$. Here we note that Eqs. (23) and (30) are the finite-volume versions of Eqs. (13) and (18) in infinite volume. Thus it is reasonable to assume that $P_{N_C^*}^V(E_k^{ave}, L)$ can be compared with $P_{N_C^*}(E)$, defined by Eq. (16), for infinite volume. This will be demonstrated explicitly in the next section.

III. ONE-CHANNEL DYNAMICAL MODEL

We first consider the dynamical Hamiltonian constructed in Ref. [33]. It has only one πN channel and one bare state $|N_C^*\rangle = |\Delta_C\rangle$ for $\Delta(3/2^+)$ in Eqs. (1) and (2). By using Eqs. (3)–(8) with $i = j = 1 = \pi N$, the πN scattering amplitudes can be calculated for each partial wave. The parameters of this model (the SL model) are determined by fitting the data for the empirical S and P partial-wave amplitudes up to invariant mass $W = 1.3$ GeV. The fits to the data are shown in Fig. 1.

The potential $v_{\pi N, \pi N}$ for this single-channel dynamical model is based on the meson-exchange mechanism. This is essential to reduce the uncertainties in determining the partial-wave amplitudes from the data, which have unavoidable systematic and statistical errors. In addition, the extracted Δ (1232) resonance parameters can be interpreted theoretically in terms of a bare state surrounded by a meson cloud.

Using the SL Hamiltonian as described above and solving Eqs. (24)–(28) with $n_c = 1$, we obtain the finite-volume
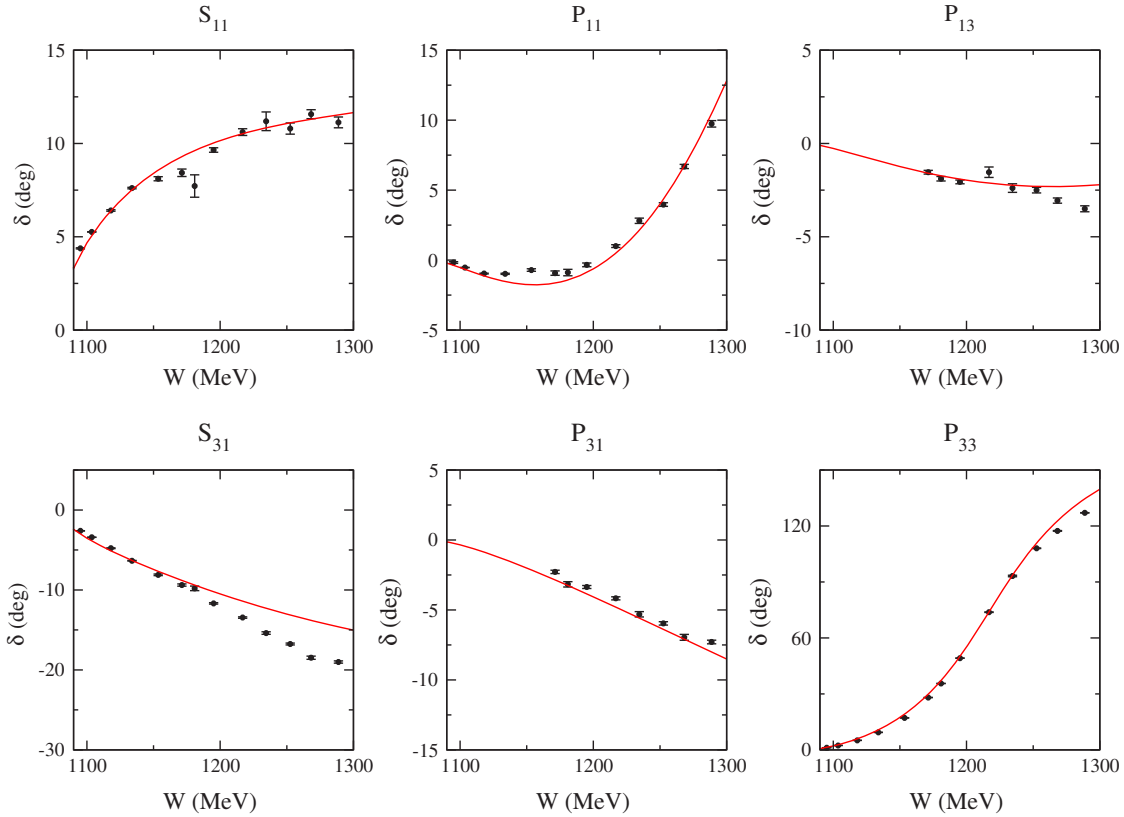
FIG. 1. Phase shifts from the SL model [33] are compared with data in the S and P partial-wave amplitudes. Panels are labeled by L_{2I2J}.

spectrum in the πN P_{33} partial wave. This finite-volume spectrum is plotted in the left-hand panel of Fig. 2 as a function of the spatial lattice length L.

With this knowledge of the finite-volume spectrum of states having the quantum numbers of the Δ, one can then use the Lüscher relation of Eq. (29) to predict the P_{33} phase shift for each of the energy levels of the predicted spectrum. These results are reported in the right-hand panel of Fig. 2 as open and full points. Open points have their origin in the finite-volume spectrum obtained at $L = 6$ fm while the full points follow from the spectrum at $L = 5$ fm as indicated in the left-hand panel of Fig. 2.
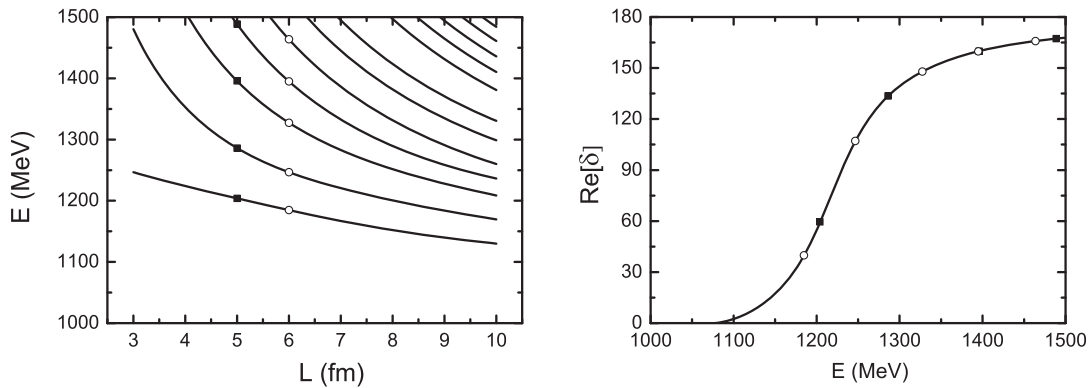
FIG. 2. Left: The finite-volume spectrum obtained via the FVH method through fits to the partial-wave scattering amplitudes plotted as a function of the spatial lattice length L. The spectrum of states obtained at $L = 5$ (full points) and 6 (open points) fm are used in the Lüscher formalism to predict the experimental phase shifts in the right-hand panel. Right: Phase shifts in the P_{33} partial wave of the πN system. Full points and open points are obtained by applying the Lüscher formalism to the finite-volume spectra of the left-hand plot at $L = 5$ and 6 fm respectively. For reference the solid curve is that of the P_{33} channel displayed in Fig. 1, obtained through the fit of the SL model [33] to the partial-wave scattering amplitudes.

For reference, the solid curve illustrated in the right-hand panel of Fig. 2 is that of the P_{33} channel displayed in Fig. 1, obtained through the fit of the SL model to the partial-wave scattering amplitudes.

We note that the phase shifts calculated from each point of the spectra at $L = 5$ and 6 fm agree with the solid curve which is consistent with the experimental values and tied to the finite-volume spectrum via the FVH model. Thus the FVH method is equivalent to the use of Lüscher's formula in relating the finite-volume spectrum to the scattering phase shifts determined by the experimental data. This is in agreement with the findings of Refs. [15,17], which used separable potentials.

The spectrum shown in the left side of Fig. 2 can be used to examine whether the experimental data, brought to the finite volume of the lattice via the SL model, is consistent with LQCD, and vice versa. However, this comparison does not necessarily test the physics considered in the formulation of the model. As demonstrated in Ref. [31], when the experimental data are complete and of very high accuracy, the predicted Δ resonance properties are independent of the model when the model(s) considered describe the data accurately. As illustrated in Fig. 1, the SL model has met this condition reasonably well.

We now turn to examine the probability, $P_{\Delta_C}(E)$ of Eq. (16) for the Δ resonance. $P_{\Delta_C}(E)$ describes the probability to find the bare Δ in the πN scattering wave function. Within the SL model, the predicted $P_{\Delta_C}(E)$ and the resonant cross section, $\sigma^{\mathrm{res}}(E)$, are compared in Fig. 3. We see that they have the same resonant structure near $E = 1232$ MeV. This is not surprising, as can be seen by comparing the expressions of Eqs. (11) and (15). The results shown in Fig. 3 indicate that the predicted $P_{\Delta_C}(E)$
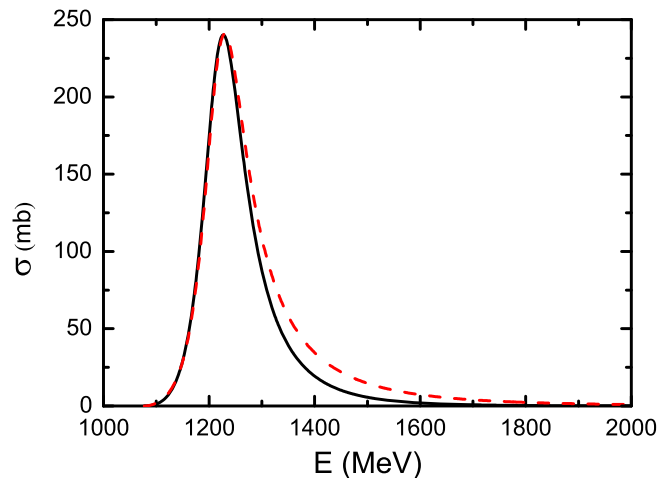
contains the information of the extracted Δ resonance projected onto the physical real-E axis.

We next use Eq. (30) to calculate $p_{\Delta_C}^V(E, L)$ which is the probability of finding the bare Δ in the eigenstate $|\Psi_E^V\rangle$ of the Hamiltonian in finite volume. We see in Fig. 4 that the calculated $p_{\Delta_C}^V(E, L)$ is not a smooth function of E for each L. As demonstrated in Appendix B within an exactly soluble model, the fluctuations are a mathematical consequence of the quantization condition in finite volume. Nevertheless, the general structure of $p_{\Delta_C}^V(E, L)$ has a resonant shape as L increases. We then find that the energy-averaged $P_{\Delta_C}^V(E, L)$, as defined by Eq. (31), is more useful as a comparison with $P_{\Delta_C}(E)$ from infinite volume. This can be seen in Fig. 5, where $P_{\Delta_C}^V(E, L)$ clearly approaches $P_{\Delta_C}(E)$ as the lattice size, L, increases.

Our results suggest that it will be interesting to calculate the analogue of $P_{N^*_C}^V(E, L)$ directly from LQCD. The formalism developed herein establishes a bridge between $P_{\Delta_C}(E)$ of the SL model in the infinite volume of experiment and the finite-volume analogue. It will be fascinating to explore the possibility of a similar quantity evaluated directly in terms of the underlying dynamics of QCD.

Obtaining a $P_{\Delta_C}^V(E, L)$ in LQCD for large L is very difficult. Nevertheless, the results shown in Fig. 5 suggest that $P_{\Delta_C}^V(E, L)$ can qualitatively reproduce the shape of $P_{\Delta_C}(E)$ even for $L = 3$ fm. We will discuss possible calculations of $P_{\Delta_C}^V(E, L)$ in Sec. V.

The authors of Refs. [36,37] also develop an approach to produce a Breit-Wigner form of resonance from the spectrum. The main differences between the two approaches are as follows. Firstly, in the approach of
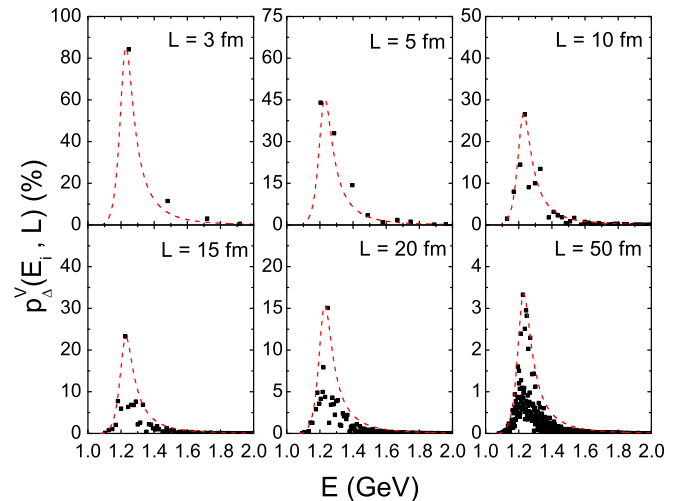

FIG. 3. Comparison of the energy dependence of the resonant cross section of πN elastic scattering in the P_{33} partial-wave channel, $\sigma^{\mathrm{res}}(E)$ (solid black curve), and the probability to find the bare Δ in the πN scattering wave function, $P_{\Delta_C}(E)$ (dashed red curve), normalized at the peak.

FIG. 4. The overlap probability, $p_{\Delta_C}^V(E_i, L) = |\langle \Delta_C | \psi^V(E_i) \rangle|^2$, of the bare Δ with the finite-volume energy eigenstate for the SL model is shown as solid square points, at $L = 3, 5, 10, 15, 20, 50$ fm. The red dashed curves show the infinite-volume $P_{\Delta_C}(E)$ normalized at the peak.
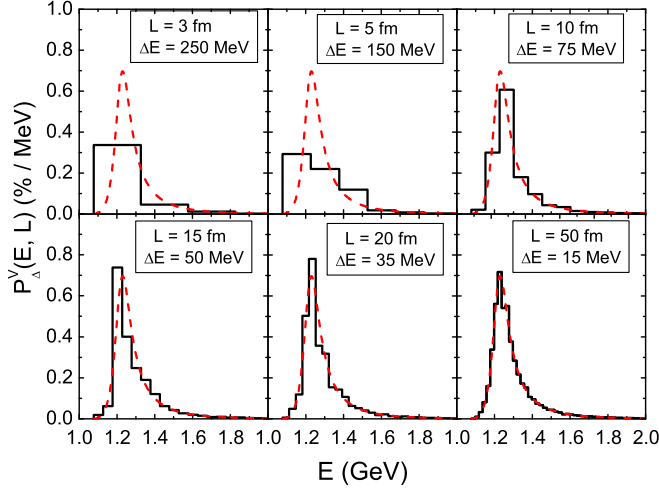
FIG. 5. The probabilities $P^V_{\Delta_C}(E, L)$ (solid black line) and $P_{\Delta_C}(E)$ (dashed red curve) of the FVH SL model at $L = 3, 5, 10, 15, 20,$ and 50 fm.

Ref. [36], they require a range of lattice sizes and the first N energy levels. However, in our approach, we only need one fixed lattice size, but all eigenstates in the considered energy range. Thus, from the practical point of view, our approach only requires results from one fixed lattice size, while the authors of Ref. [36] need results based on many different sizes. Secondly, they count the number of eigenstates in a particular momentum bin, and present a distribution based on that measure. However, in our approach, we not only count the number of eigenstates, but we also perform a summation of eigenvector coefficients. Thus, their approach makes an analysis based on eigenvalues alone, whereas our approach makes the analysis based on eigenvectors and eigenvalues. As a result, the composition of the states plays a new significant role in our analysis. Of course, when L goes to infinity in our approach, our $P^V(E, L)$ will automatically be exactly consistent with the corresponding variable $P(E)$ in the infinite volume.

IV. THREE-CHANNEL DYNAMICAL MODEL

In this section, we consider a three-channel model in the form of Eqs. (1) and (2). It includes the πN, $\pi \Delta$, and σN channels, where Δ and σ in the latter two channels are both treated as stable particles. The meson-exchange two-body interactions $v_{i,j}$ with $i, j = \pi N, \pi \Delta, \sigma N$ are taken from the ANL-Osaka Hamiltonian [32], and one bare state is included in each partial wave except for S_{11} and P_{31}. Their parameters are adjusted, along with the vertices $g_{N^*,i}$ with $i = \pi N, \pi \Delta, \sigma N$, to fit the S and P partial-wave πN empirical amplitudes [42] up to invariant mass $W = 1.6$ GeV. We see in Fig. 6 that the fits are reasonable. The only exception is the S_{11} partial wave, which is known to have a large coupling with the ηN channel and therefore cannot be fitted well in this model. Herein, we focus on the results in the P_{11} and P_{33} partial waves.
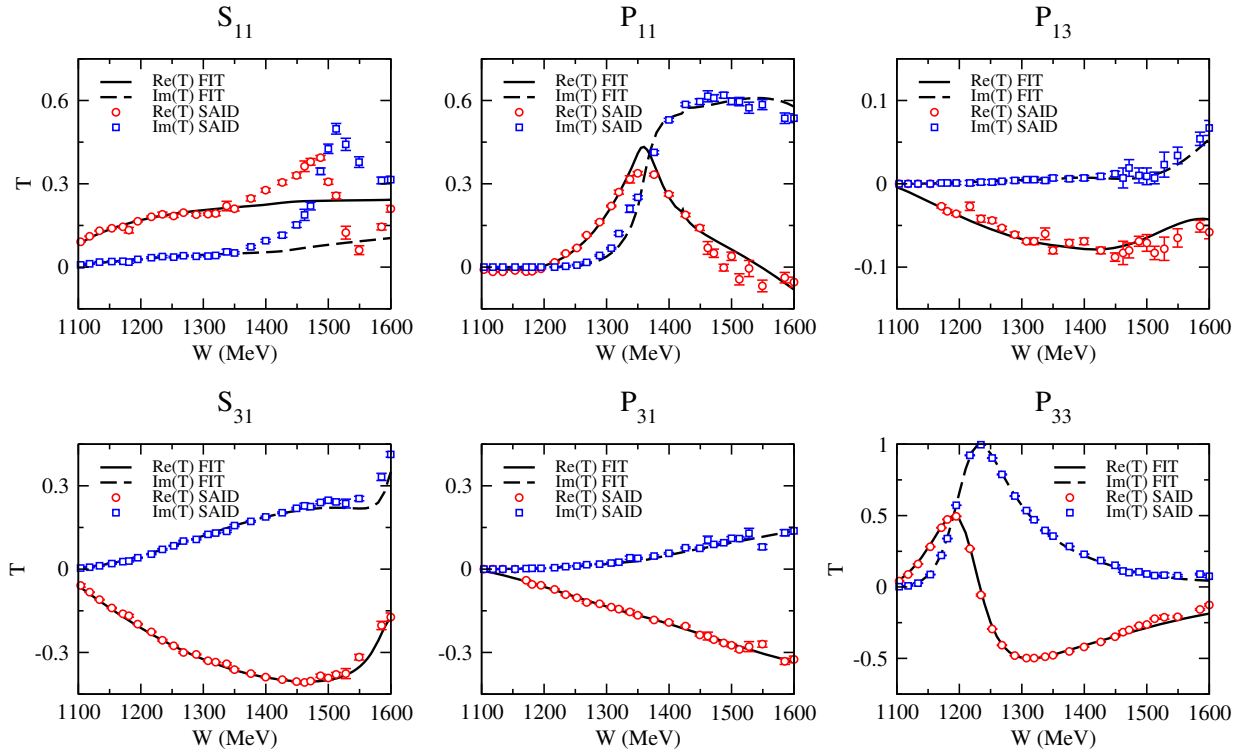

FIG. 6. Fits to the empirical data [42] for the πN partial-wave amplitudes. Panels are labeled by L_{2I2J}. With the exception of the S_{11} partial wave, where the ηN channel is required, the model describes the partial-wave amplitudes well.

By solving Eq. (24) in finite volume, we obtain the spectrum for each partial wave. The results for the P_{33} and P_{11} partial waves are shown in Fig. 7. It is interesting to note that the predicted spectrum for the P_{33} partial wave (left-hand panel) from the three-channel model agrees well with the solid squares taken from the spectrum of the single-channel SL model shown in Fig. 2. This indicates that the predicted finite-volume spectra are not sensitive to the details of the Hamiltonian provided the models agree on the predicted scattering amplitudes. This is in agreement with the findings in a study of two-channel cases in Ref. [15]. The calculated spectra for the P_{11} partial wave

are shown as the solid curves in the right-hand panel of Fig. 7.

The Lüscher formalism has been extended in Ref. [8] to the general multichannel system. By choosing the normalization to relate the T-matrix elements to S-matrix elements by $S_{\alpha,\beta}(E) = \delta_{\alpha,\beta} - 2iT_{\alpha,\beta}(E)$, the formula given in Ref. [8] for the constructed three-channel model can be written explicitly as

$$\det[M(E,L)] = 0 \tag{34}$$

where

$$M(E,L) = \begin{pmatrix} T_{\pi N,\pi N}(E) + C_{\pi N,\pi N}(L,E) & T_{\pi N,\pi\Delta}(E) & T_{\pi N,\sigma N}(E) \\ T_{\pi\Delta,\pi N}(E) & T_{\pi\Delta,\pi\Delta}(E) + C_{\pi\Delta,\pi\Delta}(L,E) & T_{\pi\Delta,\sigma N}(E) \\ T_{\sigma N,\pi N}(E) & T_{\sigma N,\pi\Delta}(E) & T_{\sigma N,\sigma N}(E) + C_{\sigma N,\sigma N}(L,E) \end{pmatrix},$$

and

$$C_{\alpha,\alpha}(L,E) = \frac{iq_\alpha(L)}{q_\alpha(L) - 4\sqrt{\pi}Z_{00}(1;q_\alpha(L))}, \tag{35}$$

and $q_\alpha(L) = k_\alpha L/(2\pi)$ is defined by the on-shell momentum k_α of total energy E in channel α.

Because of symmetries and the unitary conditions, only six of the total 12 real numbers needed to specify all six of the complex $T_{\alpha,\beta}(E)$-matrix elements are independent. Thus we need to get six relations from Eqs. (34)–(35) at each E to relate the spectrum to the scattering amplitudes shown in Fig. 6. In the rest frame, this means that we need to perform LQCD calculations at six different values of L. For $E = 1440$ MeV, this is indicated by the six solid

squares on the dashed line at the intersections of the solid curves in the left-hand panel of Fig. 7. Clearly, this constitutes an extremely difficult and time-consuming LQCD calculation. Therefore, it is hard to just apply Eq. (34) to extract the amplitude from spectra in the finite volume. In addition, for these three channels, the existing experimental data are only for the πN channel. There are no data for the other two channels. As a result, only two parameters of the six independent parameters can be extracted from data. Thus, the spectrum of the fixed size box cannot be predicated though Eq. (34) with only two inputs from the πN channel.

One possible method as described in the Introduction is to combine the Lüscher equation and a scattering model which produces the full T matrix. Because the spectra in the
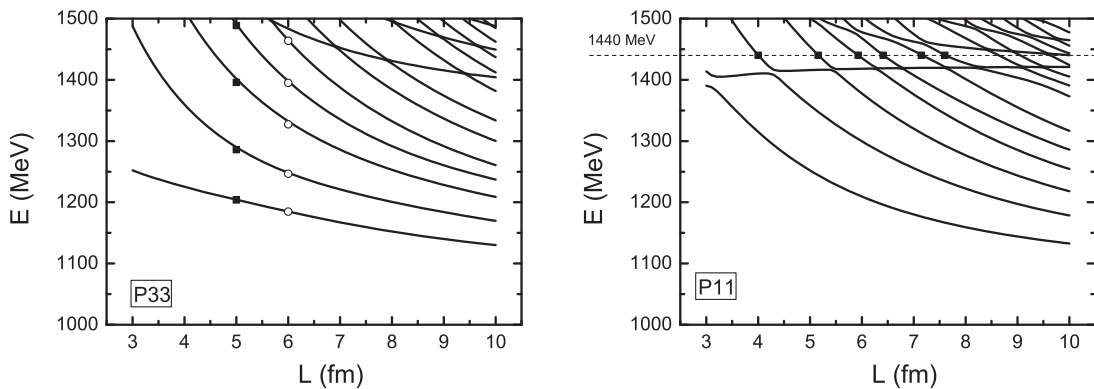

FIG. 7. The finite-volume spectra for the P_{33} (left) and P_{11} (right) partial waves, calculated from the three-channel model incorporating πN, $\pi\Delta$ and σN, plotted as a function of the spatial lattice length L. We note that the finite line width hides some of the weakly coupled avoided level crossings, particularly in the left-hand panel for the P_{33} partial wave. Avoided level crossings of the σN, πN and $\pi\Delta$ channels are readily apparent in the right-hand panel for the P_{11} partial wave. The squares in the left-hand P_{33} panel are taken from Fig. 2 for the single-channel model and illustrate the independence of the finite-volume spectrum from the model, when both models describe the empirical partial-wave scattering data well. In the right-hand panel, the six solid squares on the dashed line indicate the six lattice volumes that need to be considered in order to constrain the relations of the multichannel Lüscher formula.

TABLE I. The P_{33} and P_{11} resonance pole masses (M_R) extracted from the three-channel model. Each resonance pole mass is listed as $(\mathrm{Re}(M_R), -\mathrm{Im}(M_R))$. Experimental values are from Ref. [28]. The masses for the input bare N^* states are also listed in the third column.

L_{2I2J}	Resonance	Pole masses (MeV)	Experiment (MeV)	Bare masses (MeV)
P_{33}	$\Delta(1232)$	(1212, 53)	(1209–1211, 49–51)	1470
P_{11}	$N^*(1440)$	(1354, 38)	(1350–1380, 80–110)	2100
	$N^*(1710)$	(1717, 73)	(1670–1770, 40–190)	

finite volume can be calculated with the full T-matrix input by using the Lüscher equation, the lattice data can be fitted by the scattering model. For example, in Ref. [26], through the K-matrix model plus Lüscher equation, they successfully analyze the spectra involving the $D\pi$, $D\eta$ and $D_s\bar{K}$ channels. On the other hand, the spectrum also can be predicted just from the experimental data for the T-matrix elements of the $\pi N \to \pi N$ reaction. Firstly these data are fitted to fix the parameters in the scattering model. Secondly the scattering model produces the full T matrix. At last, the spectrum is solved by using the Lüscher equation with the full T-matrix input.

The other method is the FV Hamiltonian method used here. The parametrization of the Hamiltonian is fixed by fitting the empirical πN amplitudes [42], as shown in Fig. 6. Then one does not need to calculate the T matrix of the other two channels; the spectrum can be obtained directly from the eigenvalue of the finite-volume Hamiltonian. This spectrum can be used to test LQCD results in the physical pion mass range. If we want to get the T matrix from existing LQCD data, the parameters in the Hamiltonian can be fixed by fitting the LQCD spectrum directly. Then the fixed Hamiltonian generates the T matrix.

We now investigate the resonances extracted within this three-channel model. The extracted pole positions and bare masses are listed in Table I. The value of the resonance pole in the P_{33} channel is close to the value $M_R = 1216.4 - i\,50.0$ MeV found in the SL model [33]. This is in agreement with the finding of Ref. [31] that the resonance extraction is independent of the model, so long as the data near the resonance positions are very accurate and fitted *precisely*. This is also evident in a comparison of the P_{33} results in Figs. 2 and 6 in the region 1100 MeV $\leq W \leq$ 1250 MeV.

Turning to the P_{11} channel, we have two poles with masses $M_{R_1} = 1354.0 - i\,38.0$ MeV and $M_{R_2} = 1717.0 - i\,73.0$ MeV, located in the Riemann sheets nearest to the physical real energy axis. The situation is much more complicated in this case than for that of P_{33}. However, we find that $P_{N_C^*}(E)$ of Eq. (21), which measures the probability of finding the bare state in the meson-baryon scattering wave functions, still contains the information concerning the extracted resonances. This can be seen in Fig. 8. We find that $P_{N_C^*}(E)$ has a similar energy dependence to that of the resonant part of the elastic cross section, $\sigma^{\mathrm{res}}(E)$. In particular, the structure near $W = 1400$ MeV, reflecting the broad Roper resonance on the real axis, is also seen in $P_{N^*}(E)$.

By using the wave function, $|\Psi_E^V\rangle$, obtained by solving Eq. (24) for the three-channel Hamiltonian in finite volume, we can calculate $P_{N_C^*}^V(E, L)$ using Eq. (31). We see in Fig. 9 that the energy-averaged $P_{N_C^*}^V(E, L)$ agrees very well with $P_{N_C^*}(E)$. Thus $P_{N_C^*}(E)$ can also be used to check whether the extracted resonances are consistent with the underlying
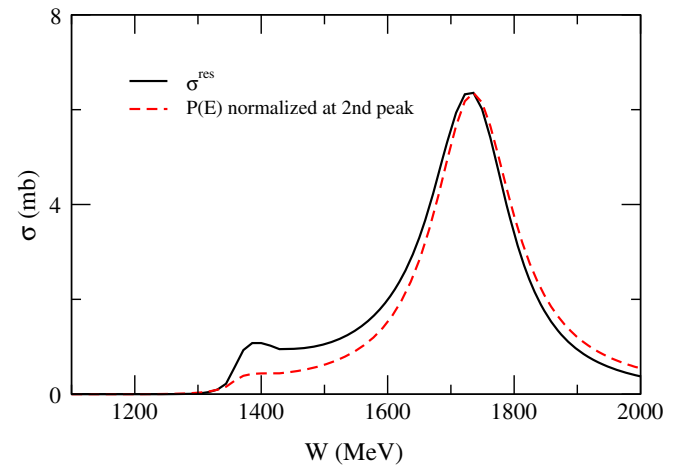
FIG. 8. Comparison of the energy dependence of σ_{res} and $P_{N_C^*}(E)$ for the P_{11} partial-wave channel, normalized at the peak.
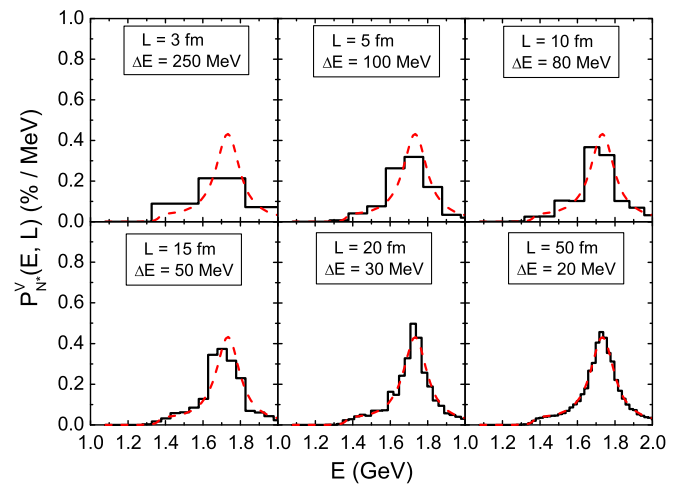
FIG. 9. The finite-volume $P_{N_C^*}^V(E, L)$ (solid black) and infinite-volume $P_{N_C^*}(E)$ (dashed red) bare-state probabilities for the three-channel model at $L = 3$, 5, 10, 15, 20, and 50 fm.

QCD dynamics, provided $P_{N_C^*}^V(E, L)$ can be calculated for sufficiently large L.

In our current model, the three-body $N\pi\pi$ channel is not included explicitly, and Δ and σ in the $\pi\Delta$ and σN channels are both introduced as stable particles. We take this approach because the treatment of three-body contributions in the finite volume is much more complicated than the two-body systems, and it remains to be solved, although there are some developments of it in Refs. [43,44]. Thus, a reasonable first step is to cast $N\pi\pi$ as $\pi\Delta$ and σN, the effects of the three-body continuum can be included in an approximate manner through the coupling to these two-body channels. While it has been argued that this approach violates unitarity in QCD and should not be used for light quark masses where the σ is unstable, we note that our approach using two-body channels maintains unitarity. Moreover, the T matrix of $\pi N \to \pi N$ is described well and the pole position is acceptable, although the imaginary part is a little far away from the PDG data as shown in Table I. This is mainly because in the considered three-channel model, the branch points of the σN and $\pi\Delta$ channels appear on the real-energy axis and thus the analytic structure of the scattering amplitude is rather different from that of the real world. We expect that the extracted P_{11} resonance pole corresponding to the Roper resonance will move to the "right" positions once the three-body $\pi\pi N$ channel effect is explicitly taken into account, while still reproducing the πN scattering phase shifts. In the future, the spectrum shown in Fig. 7 and probabilities shown in Fig. 9 should be updated by including three-body contributions.

V. LQCD CALCULATIONS OF $P_{N_C^*}^V(E, L)$

Here we explore LQCD calculations of $P_{N_C^*}^V(E, L)$ and the extent to which measures can be related to the bare states of the dynamical model. Since $P_{N_C^*}^V(E, L)$ reflects the properties of the resonance, the direct measurement of $P_{N_C^*}^V(E, L)$ from LQCD will provide the insight needed for understanding the essence of resonance structure. It holds the promise to further elucidate the effective mechanisms of QCD dynamics and extend our knowledge of QCD.

There are fundamental QCD dynamics that support the concept of a hadronic quark core dressed by a meson cloud. A particularly illustrative example is that of coherent center domains in the vacuum of QCD [45]. Within the domains governed by the trace of the Polyakov loop, color-singlet quark-antiquark pairs or three-quark triplets have a finite energy and are spatially correlated. These fundamental domains are thought to govern the size of the quark cores of hadrons [45].

Of course, there is some model dependence in the separation of an energy eigenstate into its core or bare-state contribution and its associated meson-cloud contribution. For example, in effective field theory this separation

is governed by the scale of the regulator [46,47] and in the power-counting regime of chiral perturbation theory, the physics of the expansion is independent of the regulator [48]. The physics can be shifted from the core to the cloud through a change in the regulator parameter value with no change in the renormalized low-energy coefficients. However, when working beyond the power-counting regime, an intrinsic scale reveals itself through a convergence in the values of the renormalized low-energy coefficients of the expansion [48–51]. For dipole regulators, a scale of $\sim$1 GeV is found. This intrinsic scale is associated with the finite size of the source of the meson cloud and phenomenology suggests a scale of 0.8 GeV [46,47,52–60].

With this insight, one can attribute some physics to the baryon core and the balance to the meson cloud. This approach has been very successful in correcting the meson cloud of quenched QCD to make precise full QCD predictions [52–60]. In this case the baryon core is held invariant between quenched and full QCD and the artifacts of the quenched meson cloud are removed and replaced with the full QCD cloud contribution.

In previous coupled-channel effective field theory studies of the $\Delta(1232)$ resonance it has been concluded that the $\Delta(1232)$ resonance can be interpreted as a system made of a quark core and a meson cloud. Furthermore, the contributions from the quark core to the electromagnetic $\gamma^* N \to \Delta$ form factors are found to be similar to the predictions from the three-quark configurations within either the constituent three-quark model or models based on the Dyson-Schwinger equations (DSE). Since the meson-cloud effects within the SL model are defined by well-studied meson-exchange mechanisms and are strongly constrained by fitting the πN scattering phase shifts in all partial waves, this separation of the core and meson cloud is not completely arbitrary. In summary, there is ample evidence that the essential underlying mechanism of baryon structure is that of a quark core surrounded by a meson cloud.

The results shown in Figs. 5 and 9 establish a relationship between the probabilities of finding the bare state in infinite volume, $P_{N_C^*}(E)$, and in finite volume, $P_{N_C^*}^V(E, L)$. The relationship enables a new exploration of connecting $P_{N_C^*}^V(E, L)$, containing resonance information extracted from the πN reaction data within a dynamical model, to that obtained directly from lattice QCD.

Our hypothesis is that the probability of finding the bare state in a finite-volume eigenstate of lattice QCD, $P_{N_C^*}^V(E, L)$, is related to the overlap of an appropriately smeared three-quark lattice interpolating field with the lattice QCD eigenstates. As there is some freedom in defining this three-quark operator, it will be important to examine the parameter space as one selects an operator that models the three-quark core.

For example, the spin-flavor nature of the interpolating field must be selected. For local three-quark operators, the

choice for N and Δ baryons is straightforward. The spin-flavor structure for the Δ is unique [61] and there is only one spin-1/2 nucleon operator that overlaps significantly with the nucleon and its radial excitations [62–64].

Similarly, the source of the quark propagator is smeared out to provide a finite size for the distribution of quarks within the quark core. As detailed in Appendix A, the smearing is performed in an iterative manner that gives rise to a Gaussian-shaped distribution with the size governed by the number of iterations. Radially excited cores can be constructed from a superposition of Gaussian smeared sources to create a node [63–66].

It will be interesting to examine the dependence of $P^V_{N^*_C}(E, L)$ on this smearing extent. In selecting a range of interesting values one can consider the size of the hadron as measured in form factors and draw on insight from the typical size of coherent center domains in the QCD vacuum. It is well known that smaller smearing extents have better overlap with higher excited states of the spectrum [63] and thus there is a relationship between the smearing extent and the mass of the bare state.

We note that the discrete nature of the finite-volume LQCD spectrum prevents a determination of $p^V_{N^*_C}(E, L)$ for arbitrary E. LQCD can only calculate $P^V_{N^*_C}(E_\alpha, L)$, as defined in Eq. (30), for the αth eigenstate, $|\Psi^V_{E_\alpha}\rangle$:

$$p^V_{B_C}(E_\alpha, L) = |\langle B_C | \Psi^V_{E_\alpha}\rangle|^2 \equiv |\lambda^\alpha_C|^2. \tag{36}$$

The task then is to define a bare or core state on the lattice $|B_C\rangle$. To do this we resort to the aforementioned local three-quark interpolating field, χ_C, acting on the QCD vacuum $|\Omega\rangle$. In the rest frame of the state

$$\lambda^\alpha_C u^\alpha(\vec{0}) = \langle B_C | \Psi^V_{E_\alpha}\rangle = \langle \Omega | \chi_C | \Psi^V_{E_\alpha}\rangle, \tag{37}$$

where $u^\alpha(\vec{0})$ is the zero-momentum Dirac spinor for state α. Here N^*_C and thus χ_C encode the spin, isospin and parity of the core state C under consideration. This can be the bare nucleon, bare Roper, bare $N^*(1535)$, bare Δ and so on. $|\Psi^V_{E_\alpha}\rangle$ is the αth lattice QCD eigenstate in the finite volume. As an example, consider the $[JTP] = [3/2, 3/2, +]$, Δ^{++} state where there is only one local three-quark operator transforming as a Rarita-Schwinger spinor under Lorentz transformations,

$$\chi_{C\mu}(x) = \sum_{a,b,c=1,2,3} \varepsilon^{abc}(u^{aT}(x)C\gamma_\mu u^b(x))u^c(x), \tag{38}$$

where $u^a(x)$ represents the up-quark field operator with color index a acting at space-time coordinate x. Thus, the bare state $|\Delta_C\rangle = \bar{\chi}_{C\mu}(0)|\Omega\rangle$. As such, it excites a superposition of QCD energy eigenstates governed by the smearing extent of $\chi_{C\mu}$. Our hypothesis is that this is the realization of the bare Δ^{++} in the Hamiltonian model.

The first step in evaluating λ^α_C of Eq. (36), and thus $p^V_{N^*_C}(E_\alpha, L)$, is to access the spectrum of eigenstates, $|\Psi^V_{E_\alpha}\rangle$. This is done via the variational or correlation matrix method [63–73]. The approach involves a matrix of parity-projected correlation functions. In the rest frame of the state ($\vec{p} = \vec{0}$) the correlation matrix is

$$G_{ij}(t, \vec{0}) = \sum_{\vec{x}} \mathrm{Tr}_{\mathrm{sp}}\{\Gamma_\pm \langle \Omega | \chi_i(x)\bar{\chi}_j(0)|\Omega\rangle\}. \tag{39}$$

Here, an interpolating field $\bar{\chi}_j(0)$, having the quantum numbers of the considered state, acts on the QCD vacuum $|\Omega\rangle$ and excites a superposition of finite-volume energy eigenstates. The interpolator $\bar{\chi}_j(0)$ is an arbitrary operator, constrained only by the quantum numbers. It may be a local operator or a nonlocal operator designed to provide overlap with the multiparticle scattering states of the resonance channel. For example, operators in which the momentum of each particle in the multiparticle state is specified are particularly good at exciting these states from the vacuum [68,74].

Appendix A outlines the complete details for calculating λ^α_C using the correlation matrix of Eq. (39) and the bare-state definition of Eq. (37) for $|B_C\rangle$. The final result is

$$\left(p^V_{N^*_C}(E_\alpha, L)\right)^{1/2} = \lambda^\alpha_C = z^\alpha \frac{G_{Cj}(t)u^\alpha_j}{v^\alpha_i G_{ij}(t)u^\alpha_j}. \tag{40}$$

Here the u^α_i (v^α_i) are the coefficients of the interpolating fields $\bar{\chi}_i$ (χ_i) forming the optimized interpolating fields $\bar{\phi}^\alpha = \sum u^\alpha_i \bar{\chi}_i$ ($\phi^\alpha = \sum v^\alpha_i \chi_i$), designed to isolate a single energy eigenstate, α. These coefficients are obtained by solving the generalized eigenvalue problem. The coefficients z^α are the corresponding coupling strengths between the eigenstate $|\Psi^V_{E_\alpha}\rangle$ and $\bar{\phi}^\alpha|\Omega\rangle$. In Appendix A, we provide a complete example for the nucleon case.

Finally, the averaging and normalization of Eqs. (31) and (32) respectively provide the final relations for the calculation of the energy-averaged probability $P^V_{N^*_C}(E_\alpha, L)$ from $p^V_{B_C}(E_\alpha, L)$.

In summary, a determination of $P^V_{N^*_C}(E_\alpha, L)$ in LQCD holds the potential to confirm a long-standing ansatz for the internal structure of baryon resonances in coupled-channel analyses. With regard to Figs. 5 and 9, even a volume with $L = 5$ fm should be sufficient to disclose a peak in the case of the P_{33} and P_{11} resonances. We strongly encourage LQCD groups to calculate $p^V_{B_C}(E_\alpha, L)$ in future simulations.

VI. SUMMARY AND FUTURE DEVELOPMENT

We have investigated the finite-volume Hamiltonian method by using the meson-exchange model of πN reactions within which bare states are introduced to parametrize the intrinsic excitations of the nucleon. In addition

to further examining the differences between the finite-volume Hamiltonian method and the Lüscher formalism, an approach has been developed to relate the internal structure of nucleon resonances extracted from the πN reaction data to lattice QCD (LQCD) calculations.

We first showed that the resonance pole positions can be related to the probability $P_{N_C^*}(E)$ of finding the bare state in the πN scattering states in infinite volume. We then demonstrated that the probability, $P_{N_C^*}^V(E, L)$, of finding the same bare state in the eigenstates of the underlying Hamiltonian in finite-volume approaches $P_{N_C^*}(E)$ as the volume increases. Our findings open the possibility of using $P_{N_C^*}^V(E, L)$ to examine whether the internal structure of nucleon resonances extracted from the πN reaction data within dynamical models is consistent with similar measures in LQCD.

We have also discussed possible LQCD calculations of $P_{N_C^*}^V(E, L)$ under the hypothesis that the bare states of the dynamical reaction model can be identified with spatially smeared three-quark operators acting on the nontrivial vacuum of QCD. It will be interesting to explore the results of LQCD calculations of $P_{N_C^*}^V(E, L)$.

APPENDIX A: LQCD CALCULATIONS OF $P_{N_C^*}^V(E, L)$

1. Implementation of the three-quark core

In this appendix, we use the nucleon as an example to show how to determine the three-quark core contribution to the αth eigenstate $|\lambda_C^\alpha|^2 = |\langle N_C^*|\Psi_{E_\alpha}^V\rangle|^2 = |\langle\Omega|\chi_C|\Psi_{E_\alpha}^V\rangle|^2$ as defined in Eq. (36). In practice, there is only one local

three-quark operator transforming as a spinor under Lorentz transformations that has significant overlap with the ground-state nucleon and its radial excitations,

$$\chi_C(x) = \varepsilon^{abc}(u^{aT}(x)C\gamma_5 d^b(x))u^c(x). \quad \text{(A1)}$$

Here the subscript C denotes core, indicating both the preferred spin-flavor construction of the quark core and a preferred smearing extent. By examining the overlap of this operator with the states of the spectrum, one can probe the quark-core content of the states.

On the lattice smearing proceeds in a gauge invariant manner [75] through the map

$$\psi_i(x, t) = \sum_{x'} F(x, x')\psi_{i-1}(x', t), \quad \text{(A2)}$$

where ψ is a quark spinor and

$$F(x, x') = (1 - \alpha)\delta_{x,x'}$$
$$+ \frac{\alpha}{6}\sum_{\mu=1}^3 [U_\mu(x)\delta_{x',x+\hat{\mu}} + U_\mu^\dagger(x - \hat{\mu})\delta_{x',x-\hat{\mu}}]$$

$$\text{(A3)}$$

includes the lattice gauge-field links, $U_\mu(x) = \mathcal{P}\exp\left(\int_0^a A_\mu(x + \lambda\hat{\mu})d\lambda\right)$, to maintain gauge invariance. The smearing parameter α is typically taken to be 0.7 and the smearing extent is governed by the number of smearing sweeps, n_s. Commencing with a point source in $\psi_0(x, t)$, the smeared operator is

$$\psi_{n_s}(x, t) = \sum_{x'} F^{n_s}(x, x')\psi_0(x', t). \quad \text{(A4)}$$

Typically, $n_s \sim 100$ provides optimal overlap with the ground state, corresponding to an root-mean-square (RMS) radius of 8.4 lattice units on a 32^2 lattice volume or 0.84 fm for lattice spacing $a \sim 0.1$ fm. As this optimal smearing extent includes the influence of the meson cloud, it will be interesting to explore smaller smearing extents more closely related to the quark core, governed by the presence of a coherent center domain in the QCD vacuum [45]. To accommodate the node in the radial wave function of the bare Roper, a superposition of smeared sources of different widths can be used [64].

2. Isolation of excited states

Accessing the excited states of the spectrum is done via the variational method or correlation matrix method [63–73]. The approach involves a matrix of parity-projected correlation functions. In the rest frame of the nucleon ($\vec{p} = \vec{0}$) an $N \times N$ correlation matrix provides

$$G_{ij}(t, \vec{0}) = \sum_{\vec{x}} \text{Tr}_{\text{sp}} \{ \Gamma_{\pm} \langle \Omega | \chi_i(x) \bar{\chi}_j(0) | \Omega \rangle \}. \quad (A5)$$

Here, interpolating field $\bar{\chi}_j(0)$, having the quantum numbers of the nucleon, acts on the QCD vacuum $|\Omega\rangle$ and excites a superposition of finite-volume energy eigenstates. These states are annihilated back to the vacuum at space-time x. Summing over all $\vec{x}$ projects zero momentum and taking the trace with $\Gamma_{\pm} = \frac{1}{2}(\gamma_0 \pm 1)$ projects positive/negative parity states. Upon inserting a complete set of intermediate energy eigenstates, $|\Psi_{E_\alpha}^V\rangle$, with momentum $\vec{p'}$ and spin s

$$\sum_{\alpha, \vec{p'}, s} |\Psi_{E_\alpha}^V, \vec{p'}, s\rangle \langle \Psi_{E_\alpha}^V, \vec{p'}, s| = I, \quad (A6)$$

where α can include multiparticle states, and using the space-time translation operator

$$\chi_i(x) = e^{iP \cdot x} \chi_i(0) e^{-iP \cdot x}, \quad (A7)$$

one obtains

$$G_{ij}(t, \vec{0}) = \sum_{\alpha} \sum_{s} \text{Tr}_{\text{sp}} \{ \Gamma_{\pm} \langle \Omega | \chi_i(0) | \Psi_{E_\alpha}^V, \vec{0}, s \rangle$$
$$\times \langle \Psi_{E_\alpha}^V, \vec{0}, s | \bar{\chi}_j(0) | \Omega \rangle \} e^{-E_\alpha t}, \quad (A8)$$

in Euclidean time. Recall that E_α is the energy of the eigenstate $|\Psi_{E_\alpha}^V\rangle$ at rest, i.e., m_α.

Focusing on the positive-parity sector of interest herein, the overlap of the interpolators $\chi_i(0)$ with state $|\Psi_{E_\alpha}^V, \vec{0}, s\rangle$ is described in terms of the Dirac spinor for state $\Psi_{E_\alpha}^V$, $u^\alpha(\vec{0}, s)$, as

$$\langle \Omega | \chi_i(0) | \Psi_{E_\alpha}^V, \vec{0}, s \rangle = \lambda_i^\alpha u^\alpha(\vec{0}, s), \quad (A9)$$

and

$$\langle \Psi_{E_\alpha}^V, \vec{0}, s | \bar{\chi}_j(0) | \Omega \rangle = \bar{\lambda}_j^\alpha \bar{u}^\alpha(\vec{0}, s). \quad (A10)$$

Here, λ_i^α and $\bar{\lambda}_j^\alpha$ are the couplings of interpolators χ_i and $\bar{\chi}_j$ at the sink and source respectively to eigenstates $\alpha = 0, \ldots, (N-1)$. Recalling

$$\sum_s u^\alpha(\vec{p}, s) \bar{u}^\alpha(\vec{p}, s) = \frac{\gamma \cdot p + m_\alpha}{2\sqrt{m_\alpha^2 + \vec{p}^2}}, \quad (A11)$$

and taking the spinor trace, the two-point function takes the form

$$G_{ij}(t, \vec{0}) = \sum_{\alpha=0}^{N-1} \lambda_i^\alpha \bar{\lambda}_j^\alpha e^{-m_\alpha t}. \quad (A12)$$

The interpolating fields provide an N-dimensional basis upon which to describe the N lowest-lying states.

Using this basis, we seek linear combinations which isolate each state, α,

$$\bar{\phi}^\alpha = \sum_{i=1}^{N} u_i^\alpha \bar{\chi}_i, \quad \phi^\alpha = \sum_{i=1}^{N} v_i^\alpha \chi_i, \quad (A13)$$

such that

$$\langle \Psi_{E_\beta}^V, \vec{p}, s | \bar{\phi}^\alpha | \Omega \rangle = \delta_{\alpha\beta} \bar{z}^\alpha \bar{u}^\alpha(\vec{p}, s),$$
$$\text{and} \quad \langle \Omega | \phi^\alpha | \Psi_{E_\beta}^V, \vec{p}, s \rangle = \delta_{\alpha\beta} z^\alpha u^\alpha(\vec{p}, s). \quad (A14)$$

Here z^α and $\bar{z}^\alpha$ are the coupling strengths of ϕ^α and $\bar{\phi}^\alpha$ to the state $|\Psi_{E_\alpha}^V, \vec{p}, s\rangle$.

By multiplying the correlation matrix $G_{ij}(t)$ by u_j^α and summing over repeated indices, one obtains

$$G_{ij}(t, \vec{0}) u_j^\alpha = \sum_{\vec{x}} \text{Tr}_{\text{sp}} \{ \Gamma_{\pm} \langle \Omega | \chi_i(x) \bar{\chi}_j(0) u_j^\alpha | \Omega \rangle \}, \quad (A15a)$$

$$= \sum_{\vec{x}} \text{Tr}_{\text{sp}} \{ \Gamma_{\pm} \langle \Omega | \chi_i(x) \bar{\phi}_j(0) | \Omega \rangle \}, \quad (A15b)$$

$$= \lambda_i^\alpha \bar{z}^\alpha e^{-m_\alpha t}, \quad (A15c)$$

illustrating that the time dependence is described by the mass of the eigenstate energy. Since the t dependence is described by the exponential term alone, a recurrence relation at times t and $t + \Delta t$ constructed

$$G_{ij}(t + \Delta t) u_j^\alpha = e^{-m_\alpha \Delta t} G_{ij}(t) u_j^\alpha. \quad (A16)$$

This generalized eigenvalue equation can be solved for eigenvectors $\mathbf{u}^\alpha$ with eigenvalues $\exp(-m_\alpha \Delta t)$. Similarly

$$v_i^\alpha G_{ij}(t + \Delta t) = e^{-m_\alpha \Delta t} v_i^\alpha G_{ij}(t) \quad (A17)$$

defines the left eigenvector $\mathbf{v}^\alpha$. With the eigenvectors normalized in the usual manner $\mathbf{u}^{\dagger\alpha} \mathbf{u}^\alpha = \mathbf{v}^{\dagger\alpha} \mathbf{v}^\alpha = 1$, the coupling strengths z^α and $\bar{z}^\alpha$ are defined.

The eigenvectors u_j^α and v_i^α can then be used to create the projected correlator

$$v_i^\alpha G_{ij}(t) u_j^\beta = \delta^{\alpha\beta} z^\alpha \bar{z}^\beta e^{-m_\alpha t}. \quad (A18)$$

In the ensemble average the correlation matrix is symmetric and therefore one usually works with the improved unbiased estimator $(G_{ij}(t) + G_{ji}(t))/2$. Because the QCD action is the same for link ensembles $\{U_\mu(x)\}$ and $\{U_\mu^*(x)\}$ one can show that the two-point correlation functions of the correlation matrix can be made to be perfectly real [76–78]. Averaging the link ensembles $\{U_\mu(x)\}$ and $\{U_\mu^*(x)\}$ and ensuring that G is symmetric for each configuration ensures that the coupling strengths are real and $\bar{\lambda}_i^\alpha = \lambda_i^\alpha$ and $\bar{z}^\alpha = z^\alpha$.

3. Determining the strength of the core

We are now in a position to determine the overlap of lattice-QCD energy eigenstate $|\Psi_{E_\alpha}^V\rangle$ with the three-quark core, $\langle N_C^*|\Psi_{E_\alpha}^V\rangle$. Using the projected correlator of Eq. (A18) the overlap of the eigenstate interpolators ϕ^α and $\bar\phi^\alpha$ is determined by a linear fit to the logarithm of the projected correlator

$$\log\left(v_i^\alpha G_{ij}(t)u_j^\alpha\right) = 2\log(z^\alpha) - m_\alpha t. \qquad (A19)$$

The core contribution can be isolated via Eqs. (A15b) and (A15c). Replacing $\langle\Omega|\chi_i(x)$ by the core contribution $\langle\Omega|\chi_C(x) = \langle N_C^*|$, the core contribution to eigenstate $|\Psi_{E_\alpha}^V\rangle$, $\langle N_C^*|\Psi_{E_\alpha}^V\rangle = \lambda_C^\alpha$, is obtained via

$$\log(G_{Cj}(t)u_j^\alpha) = \log(\lambda_C^\alpha) + \log(z^\alpha) - m_\alpha t, \qquad (A20)$$

where

$$G_{Cj}(t) = \sum_{\vec{x}}\mathrm{Tr}_{\mathrm{sp}}\{\Gamma_{\pm}\langle\Omega|\chi_C(x)\bar\chi_j(0)|\Omega\rangle\}. \qquad (A21)$$

Here the time dependence can be eliminated through a ratio such that

$$\lambda_C^\alpha = z^\alpha\frac{G_{Cj}(t)u_j^\alpha}{v_i^\alpha G_{ij}(t)u_j^\alpha}. \qquad (A22)$$

APPENDIX B: THE STUDY OF FLUCTUATION OF $p_\Delta^V(E)$

To understand the fluctuation of $p_\Delta^V(E, L)$ shown in Fig. 4, we consider an exactly soluble model which has one bare state and one channel ($1b1c$) to describe the P_{33} πN
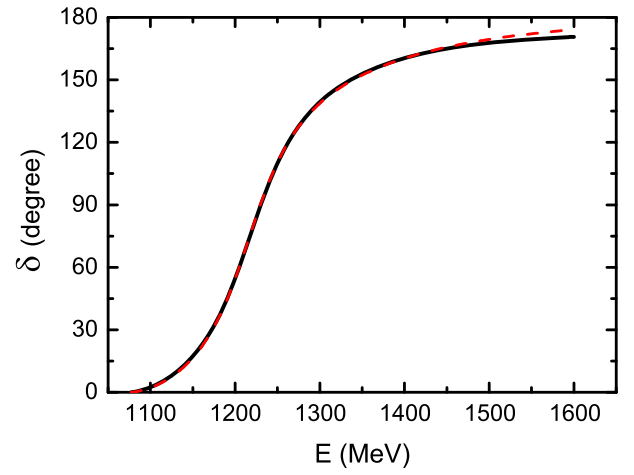

FIG. 10. The solid black and dashed red lines are calculated from the SL model and $1b1c$ model, respectively.

scattering. The Hamiltonian of this $1b1c$ model only has a bare $\Delta \to \pi N$ interaction:

$$\Gamma(k) \equiv \langle k|g|\Delta\rangle$$

$$= \frac{g}{\sqrt{m_\pi}}\frac{k}{\sqrt{m_\pi^2 + k^2}}\frac{1}{(1 + (k/\Lambda)^2)^2}\frac{1}{\sqrt{1 + (k/\Lambda)^2}},$$

$$(B1)$$

where g and Λ are the bare coupling and cutoff, and m_π is the mass of the pion. As shown in Fig. 10, the P_{33} phase shifts generated from the SL model can be reproduced by choosing $g = 0.30390$, $\Lambda = 656.60$ MeV, and $m_0 = 1265.04$ MeV for the mass of the bare Δ.

Within this $1b1c$ model, we need to find the eigenvalues E_i and eigenstate $|\Psi^V(E_i)\rangle$ from the Hamiltonian matrix of the following form:

$$[H]_{N+1} = \begin{pmatrix} m_0 & g^V(k_0) & g^V(k_1) & \cdots & g^V(k_{N-1}) \\ g^V(k_0) & E_\pi(k_0) + E_N(k_0) & 0 & \cdots & 0 \\ g^V(k_1) & 0 & E_\pi(k_1) + E_N(k_1) & \cdots & 0 \\ \vdots & \vdots & \vdots & \ddots & \vdots \\ g^V(k_{N-1}) & 0 & 0 & \cdots & E_\pi(k_{N-1}) + E_N(k_{N-1}) \end{pmatrix},$$

where $k_n = \sqrt{n}2\pi/L$ for integers $n = 0, 1, 2\ldots$, as specified by the quantization condition in finite volume with size L, and

$$g^V(k_n) = \sqrt{\frac{C_3(n)}{4\pi}}\left(\frac{2\pi}{L}\right)^{3/2}\Gamma(k_n). \qquad (B2)$$

Here $C_3(n)$ is the number of degenerate states with the same magnitude, $k_n = |\vec{k}_n|$.

With the simple matrix $[H]_{N+1}$ given above, it is easy to see that Eq. (24) for finding the eigenvalues becomes
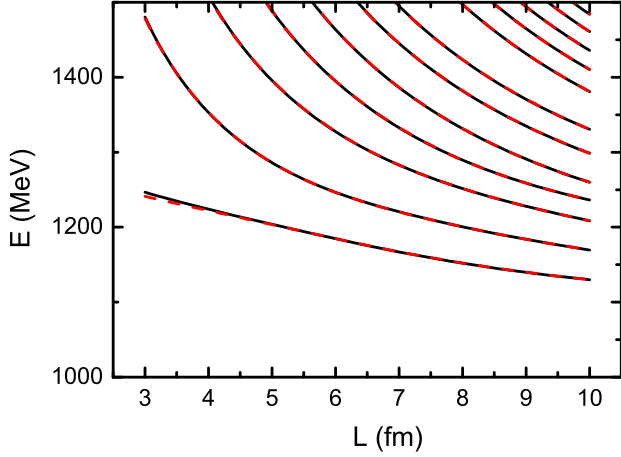
$$E_i - m_0 - \Sigma^V(E_i, L) = 0, \qquad (B3)$$

FIG. 11. The spectrum of πN in the finite volume. The solid black and dashed red lines are calculated from the SL model and $1b1c$ model, respectively.
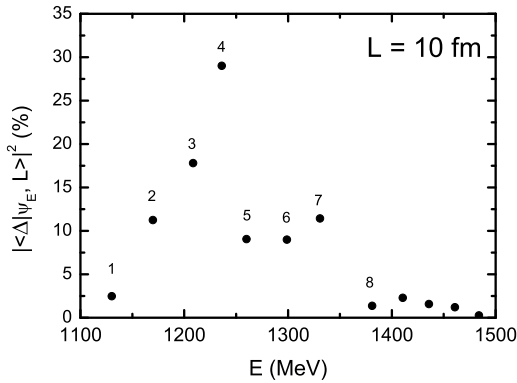
where the self-energy is

$$\Sigma^V(E,L) \equiv \sum_n \left(\frac{2\pi}{L}\right)^3 \frac{C_3(n)}{4\pi} \frac{\Gamma(k_n)\Gamma^*(k_n)}{E - E_\pi(k_n) - E_N(k_n)}.$$

(B4)

The solutions of Eq. (B3) reproduce the spectrum of the SL model, as shown in Fig. 11. The eigenstate $|\Psi^V(E_i)\rangle$ can also be solved exactly:

$$|\Psi^V(E_i)\rangle = \frac{1}{\sqrt{Z(E_i,L)}} \left[|\Delta\rangle + \sum_n \sqrt{\frac{C(n)}{4\pi}} \left(\frac{2\pi}{L}\right)^{\frac{3}{2}} \right.$$
$$\left. \times \frac{\Gamma(k_n)}{E_i - E_\pi(k_n) - E_N(k_n)} |k_n\rangle \right],$$

(B5)

where the normalization constant is

$$Z(E_i,L) = 1 + \sum_n \left(\frac{2\pi}{L}\right)^3 \frac{C(n)}{4\pi} \frac{\Gamma^*(k_n)\Gamma(k_n)}{(E_i - E_\pi(k_n) - E_N(k_n))^2}.$$

(B6)

From Eqs. (B4) and (B6), we have the following relation:

$$Z(E_i,L) = 1 - \left.\frac{\partial \Sigma^V(E,L)}{\partial E}\right|_{E=E_i}.$$

(B7)

From Eqs. (B5) and (B6), we then have

$$p_{\Delta_C}^V(E_i,L) = |\langle \Delta_C | \Psi^V(E_i)\rangle|^2 = \frac{1}{Z(E_i,L)}$$

$$= \frac{1}{1 - \frac{\partial \Sigma^V(E,L)}{\partial E}|_{E=E_i}}.$$

(B8)

The results of $p_{\Delta_C}^V(E_i,L)$ for various volume sizes L are similar to those shown in Fig. 4 for the SL model. Here we only show the result of $L = 10$ fm in the left side of Fig. 12.

Obviously, $p_{\Delta_C}^V(E_i,L)$ also shows fluctuations within this exactly soluble $1b1c$ model. To understand this, we show $\Sigma^V(E_i,L)$ (solid black curves) and $E - m_0$ (dashed red line) in the right-hand panel of Fig. 12. From Eq. (B3), it is obvious that the ith solid green dot in the right side is the eigenvalue E_i for each $p_\Delta^V(E_i,L)$ shown in the left side of the figure. From the expression Eq. (B6), we see that when an eigenvalue E_i is close to any of the energy grid points, $\epsilon(k_n) \equiv E_\pi(k_n) + E_N(k_n)$, the normalization constant $Z(E_i,L) \to \infty$ and hence $p_{\Delta_C}^V(E_i,L)$, as defined in Eq. (B8), becomes negligible. It is also clear that if E_i is farther away from the energy grid points, $Z(E_i,L)$ will be smaller and hence $p_{\Delta_C}^V(E_i,L)$ will be larger. We can see this clearly by comparing the values of $p_{\Delta_C}^V(E_i,L)$ (black dots in the left side) for the first to fourth eigenvalues and the distances between the corresponding green dots and the
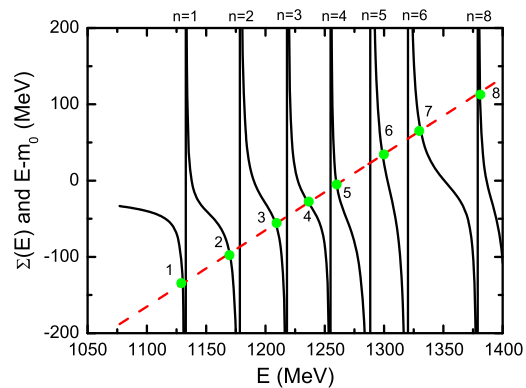

FIG. 12. Left: $|\langle\Delta_C|\Psi^V(E_i)\rangle|^2$ vs E_i at $L = 10$ fm. Right: Functions $\Sigma^V(E)$ (solid black line) and $E - m_0$ (dashed red line) as a function of energy E. The solid green points are the crossing points of the black and red lines, corresponding to the eigenvalues of the Hamiltonian.

TABLE II. The value of $-\frac{\partial \Sigma^V(E)}{\partial E}\big|_{E=E_i}$ in the $1b1c$ model.

i	E_i (MeV)	$-\frac{\partial \Sigma^V(E)}{\partial E}\big|_{E=E_i}$
1	1130.1	38.8
2	1169.7	7.88
3	1208.5	4.51
4	1236.2	2.45
5	1260.0	10.1
6	1298.8	10.2
7	1330.8	7.70
8	1381.0	75.9

nearest energy grid points on the right side. Similar comparisons also explain the fluctuation between the fourth and eighth eigenvalues. The peak at the seventh eigenvalue in the left side can be understood as follows. The gap between two grid energies near the seventh eigenvalue is much larger than the distances between any other two energy grids, since there is no integer vector which has a length equal to $\sqrt{7}$. As a result, the self-energy $\Sigma^V(E, L)$ has a smaller slope near the seventh eigenvalue and hence $-\frac{\partial \Sigma^V(E,L)}{\partial E}\big|_{E=E_7}$ is smaller than those of the sixth and eighth eigenvalues. This can be seen in Table II. The fluctuations in other areas can also be understood from Eq. (B8) and the values listed in Table II.

In summary, the fluctuation in $p_{\Delta_C}^V(E_i, L)$ is the mathematical consequence of the special property of the lattice momenta specified by the quantization condition in finite volume. While this can be proved unambiguously only within this exactly soluble $1b1c$ model, it does provide an explanation for the fluctuations seen in Fig. 4 for the more realistic SL model.

[1] C. Alexandrou, J. Phys. Conf. Ser. **562**, 012007 (2014).
[2] R. Edwards, Proc. Sci., CD15 (**2016**) 012.
[3] M. Luscher, Commun. Math. Phys. **105**, 153 (1986).
[4] M. Lüscher, Nucl. Phys. **B354**, 531 (1991).
[5] K. Rummukainen and S. A. Gottlieb, Nucl. Phys. **B450**, 397 (1995).
[6] C. H. Kim, C. T. Sachrajda, and S. R. Sharpe, Nucl. Phys. **B727**, 218 (2005).
[7] S. He, X. Feng, and C. Liu, J. High Energy Phys. 07 (2005) 011.
[8] M. T. Hansen and S. R. Sharpe, Phys. Rev. D **86**, 016007 (2012).
[9] R. A. Briceno, Z. Davoudi, and T. Luu, Phys. Rev. D **88**, 034502 (2013).
[10] M. Gockeler, R. Horsley, M. Lage, U.-G. Meissner, P. E. L. Rakow, A. Rusetsky, G. Schierholz, and J. M. Zanotti, Phys. Rev. D **86**, 094513 (2012).
[11] R. A. Briceno, Phys. Rev. D **89**, 074507 (2014).
[12] D. Mohler, Proc. Sci., LATTICE2012 (**2012**) 003.
[13] P. Guo, J. Dudek, R. Edwards, and A. P. Szczepaniak, Phys. Rev. D **88**, 014501 (2013).
[14] J. J. Dudek, R. G. Edwards, C. E. Thomas, and D. J. Wilson (Hadron Spectrum Collaboration), Phys. Rev. Lett. **113**, 182001 (2014); J. J. Dudek, R. G. Edwards, and D. J. Wilson, Phys. Rev. D **93**, 094506 (2016).
[15] J.-J. Wu, T.-S. H. Lee, A. W. Thomas, and R. D. Young, Phys. Rev. C **90**, 055206 (2014).
[16] D. J. Wilson, R. A. Briceno, J. J. Dudek, R. G. Edwards, and C. E. Thomas, Phys. Rev. D **92**, 094502 (2015).
[17] J. M. M. Hall, A. C.-P. Hsu, D. B. Leinweber, A. W. Thomas, and R. D. Young, Phys. Rev. D **87**, 094510 (2013).
[18] J. M. M. Hall, W. Kamleh, D. B. Leinweber, B. J. Menadue, B. J. Owen, A. W. Thomas, and R. D. Young, Phys. Rev. Lett. **114**, 132002 (2015).
[19] Z. W. Liu, W. Kamleh, D. B. Leinweber, F. M. Stokes, A. W. Thomas, and J. J. Wu, Phys. Rev. Lett. **116**, 082004 (2016).
[20] Z. W. Liu, W. Kamleh, D. B. Leinweber, F. M. Stokes, A. W. Thomas, and J. J. Wu, Phys. Rev. D **95**, 034034 (2017).
[21] Z. W. Liu, J. M. M. Hall, D. B. Leinweber, A. W. Thomas, and J. J. Wu, Phys. Rev. D **95**, 014506 (2017).
[22] M. Döring, U.-G. Meissner, E. Oset, and A. Rusetsky, Eur. Phys. J. A **47**, 139 (2011).
[23] M. Döring, U.-G. Meissner, E. Oset, and A. Rusetsky, Eur. Phys. J. A **48**, 114 (2012).
[24] A. M. Torres, L. R. Dai, C. Koren, D. Jido, and E. Oset, Phys. Rev. D **85**, 014027 (2012); M. Döring and U.-G. Meissner, J. High Energy Phys. 01 (2012) 009; M. Döring, M. Mai, and U.-G. Meissner, Phys. Lett. B **722**, 185 (2013).
[25] L. S. Geng, X. L. Ren, Y. Zhou, H. X. Chen, and E. Oset, Phys. Rev. D **92**, 014029 (2015).
[26] G. Moir, M. Peardon, S. M. Ryan, C. E. Thomas, and D. J. Wilson, J. High Energy Phys. 10 (2016) 011.
[27] J. J. Dudek, R. G. Edwards, and D. J. Wilson (Hadron Spectrum Collaboration), Phys. Rev. D **93**, 094506 (2016).
[28] K. A. Olive et al. (Particle Data Group Collaboration), Chin. Phys. C **38**, 090001 (2014).
[29] S. R. Beane, E. Chang, S. D. Cohen, W. Detmold, H.-W. Lin, T. C. Luu, K. Orginos, A. Parreño, M. J. Savage, and A. Walker-Loud (NPLQCD Collaboration), Phys. Rev. Lett. **109**, 172001 (2012).
[30] A. M. Sandorfi, S. Hoblit, H. Kamano, and T.-S. H. Lee, J. Phys. G **38**, 053001 (2011); M. Lüscher, Nucl. Phys. **B354**, 531 (1991).
[31] T.-S. H. Lee, J.-J. Wu, and H. Kamano, Few-Body Syst. **57**, 883 (2016).
[32] H. Kamano, S. X. Nakamura, T.-S. H. Lee, and T. Sato, Phys. Rev. C **88**, 035209 (2013); **94**, 015201 (2016).

[33] T. Sato and T.-S. H. Lee, Phys. Rev. C **54**, 2660 (1996); **63**, 055201 (2001); B. Juliá-Díaz, T.-S. H. Lee, T. Sato, and L. C. Smith, Phys. Rev. C **75**, 015205 (2007).

[34] S. Theberge, A. W. Thomas, and G. A. Miller, Phys. Rev. D **22**, 2838 (1980); **23**, 2106(E) (1981).

[35] A. W. Thomas, Adv. Nucl. Phys. **13**, 1 (1984).

[36] V. Bernard, M. Lage, U. G. Meissner, and A. Rusetsky, J. High Energy Phys. 08 (2008) 024.

[37] P. Giudice, D. McManus, and M. Peardon, Phys. Rev. D **86**, 074516 (2012).

[38] N. Suzuki, T. Sato, and T.-S. H. Lee, Phys. Rev. C **79**, 025205 (2009).

[39] N. Suzuki, B. Julia-Diaz, H. Kamano, T.-S. H. Lee, A. Matsuyama, and T. Sato, Phys. Rev. Lett. **104**, 042302 (2010).

[40] A. Bohm, *Quantum Mechanics: Foundations and Applications* (Springer-Verlag, New York, 1993).

[41] M. L. Goldberger and K. M. Watson, *Collision Theory* (Robert E. Krieger Publishing Company, Inc., New York, 1975).

[42] CNS Data Analysis Center, George Washington University, http://gwdac.phys.gwu.edu.

[43] M. T. Hansen and S. R. Sharpe, Phys. Rev. D **90**, 116003 (2014).

[44] M. T. Hansen and S. R. Sharpe, Phys. Rev. D **92**, 114509 (2015).

[45] F. M. Stokes, W. Kamleh, and D. B. Leinweber , Ann. Phys. (Amsterdam) **348**, 341 (2014).

[46] R. D. Young, D. B. Leinweber, and A. W. Thomas, Prog. Part. Nucl. Phys. **50**, 399 (2003).

[47] D. B. Leinweber, A. W. Thomas, and R. D. Young, Phys. Rev. Lett. **92**, 242002 (2004).

[48] J. M. M. Hall, D. B. Leinweber, and R. D. Young, Phys. Rev. D **82**, 034010 (2010).

[49] J. M. M. Hall, D. B. Leinweber, and R. D. Young, Phys. Rev. D **85**, 094502 (2012).

[50] J. M. M. Hall, D. B. Leinweber, B. J. Owen, and R. D. Young, Phys. Lett. B **725**, 101 (2013).

[51] J. M. M. Hall, D. B. Leinweber, and R. D. Young, Phys. Rev. D **88**, 014504 (2013).

[52] R. D. Young, D. B. Leinweber, A. W. Thomas, and S. V. Wright, arXiv:hep-lat/0111041.

[53] R. D. Young, D. B. Leinweber, A. W. Thomas, and S. V. Wright, Phys. Rev. D **66**, 094507 (2002).

[54] D. B. Leinweber, S. Boinepalli, I. C. Cloet, A. W. Thomas, A. G. Williams, R. D. Young, J. M. Zanotti, and J. B. Zhang, Phys. Rev. Lett. **94**, 212001 (2005).

[55] D. B. Leinweber, S. Boinepalli, A. W. Thomas, A. G. Williams, R. D. Young, J. B. Zhang, and J. M. Zanotti, Eur. Phys. J. A **24**, 79 (2005).

[56] D. B. Leinweber, S. Boinepalli, A. W. Thomas, P. Wang, A. G. Williams, R. D. Young, J. M. Zanotti, and J. B. Zhang, Phys. Rev. Lett. **97**, 022001 (2006).

[57] P. Wang, D. B. Leinweber, A. W. Thomas, and R. D. Young, Phys. Rev. D **75**, 073012 (2007).

[58] P. Wang, D. B. Leinweber, A. W. Thomas, and R. D. Young, Phys. Rev. C **79**, 065202 (2009).

[59] P. Wang, D. B. Leinweber, A. W. Thomas, and R. D. Young, Phys. Rev. D **86**, 094038 (2012).

[60] P. Wang, D. B. Leinweber, and A. W. Thomas, Phys. Rev. D **89**, 033008 (2014).

[61] Y. Chung, H. G. Dosch, M. Kremer, and D. Schall, Nucl. Phys. **B197**, 55 (1982).

[62] D. B. Leinweber, Phys. Rev. D **51**, 6383 (1995).

[63] M. S. Mahbub, W. Kamleh, D. B. Leinweber, P. J. Moran, and A. G. Williams (CSSM Lattice Collaboration), Phys. Lett. B **707**, 389 (2012).

[64] M. S. Mahbub, W. Kamleh, D. B. Leinweber, P. J. Moran, and A. G. Williams, Phys. Rev. D **87**, 094506 (2013).

[65] D. S. Roberts, W. Kamleh, and D. B. Leinweber, Phys. Lett. B **725**, 164 (2013).

[66] D. S. Roberts, W. Kamleh, and D. B. Leinweber, Phys. Rev. D **89**, 074501 (2014).

[67] R. G. Edwards, J. J. Dudek, D. G. Richards, and S. J. Wallace, Phys. Rev. D **84**, 074508 (2011).

[68] C. B. Lang and V. Verduci, Phys. Rev. D **87**, 054502 (2013).

[69] C. Michael, Nucl. Phys. **B259**, 58 (1985).

[70] M. Luscher and U. Wolff, Nucl. Phys. **B339**, 222 (1990).

[71] C. McNeile and C. Michael (UKQCD Collaboration), Phys. Rev. D **63**, 114503 (2001).

[72] C. Alexandrou, T. Korzec, G. Koutsou, and T. Leontiou, Phys. Rev. D **89**, 034502 (2014).

[73] A. L. Kiratidis, W. Kamleh, D. B. Leinweber, and B. J. Owen, Phys. Rev. D **91**, 094509 (2015).

[74] C. B. Lang, L. Leskovec, M. Padmanath, and S. Prelovsek, Phys. Rev. D **95**, 014510 (2017).

[75] S. Gusken, Nucl. Phys. B, Proc. Suppl. **17**, 361 (1990).

[76] T. Draper, R. M. Woloshyn, W. Wilcox, and K. F. Liu, Nucl. Phys. B, Proc. Suppl. **9**, 175 (1989).

[77] D. B. Leinweber, R. M. Woloshyn, and T. Draper, Phys. Rev. D **43**, 1659 (1991).

[78] S. Boinepalli, D. B. Leinweber, A. G. Williams, J. M. Zanotti, and J. B. Zhang, Phys. Rev. D **74**, 093005 (2006).